REVIEW ARTICLE

PCCP
www.rsc.org/pccp

# Quasielastic neutron scattering and relaxation processes in proteins: analytical and simulation-based models†

**Gerald R. Kneller*[ab]**

[a] *Laboratoire Léon Brillouin, CEA Saclay, 91191 Gif-sur-Yvette, France. E-mail: kneller@llb.saclay.cea.fr; kneller@cnrs-orleans.fr*
[b] *Centre de Biophysique Moléculaire, CNRS‡, Rue Charles Sadron, 45071 Orléans, France*

***Received 8th February 2005, Accepted 27th April 2005***
***First published as an Advance Article on the web 1st June 2005***

The present article gives an overview of analytical and simulation approaches to describe the relaxation dynamics of proteins. Particularly emphasised are recent developments of theoretical models, such as fractional Brownian dynamics. The latter connects dynamical events seen on the pico- to nanoscond time scale, accessible to quasielastic neutron scattering, and functional dynamics of proteins on much longer time scales.

## I. Introduction

There is now ample evidence that the internal dynamics of proteins is as closely related to their function as their folded structure. Using single molecule fluorescence photon correlation spectroscopy (FCS), Xie and coworkers demonstrated this recently by following the functional dynamics of a protein in real time.[1] The study revealed that functional dynamics of a protein takes place on time scales which are comparable to those required for protein folding: *i.e.* on time scales in the millisecond to second range. Nevertheless a correlation between the dynamics and the function of a protein can also be seen with spectroscopic techniques which give access to fast motions in a protein, such as elastic and quasielastic scattering of thermal neutrons (QENS). Using elastic incoherent neutron scattering Ferrand *et al.* found for example[2] that the function of bacteriorhodopsin is correlated with a dynamical transition, the so-called "glass transition", at about 200 K, which is also seen for other proteins, such as myoglobin,[3] superoxide dismutase,[4] and α-amylase.[5] The dynamical transition is characterised by the onset of stochastic motions which are absent at low temperatures, where the internal dynamics of proteins is dominated by harmonic vibrations. At the same time the atomic fluctuations increase much more rapidly with temperature than below the transition temperature, indicating an increased flexibility of the protein. The transition from one regime to the other is not very sharp, but takes place over a temperature range of a few 10 K. It depends crucially on the environmental conditions, such as membrane hydration and solvent.[2,6–8]

Using the simple mechanical model of a harmonic oscillator, Zaccai proposed to relate protein function to an effective internal force constant which describes the internal flexibility or "resilience" of a protein.[9] Such a model can describe the position fluctuations seen by elastic neutron scattering below and above the glass transition. No extension of this quite successful simple model has been proposed to include also the description of the stochastic internal dynamics which is seen by quasielastic neutron scattering (QENS). The reason might be that a harmonic potential is often associated with vibrational motions and not with stochastic motions, as they are seen by QENS. Many QENS studies have been devoted to the study of protein dynamics as a function of hydration at ambient temperature,[6,7,10–14] and are usually interpreted in terms of the model by Volino and Dianoux of Brownian motion in a spherical cavity.[15] This model accounts for the confinement of atomic motions in proteins, but cannot describe the empirical fact that correlation functions related to internal protein dynamics exhibit long-time memory effects leading to strongly non-exponentially decaying correlation functions. These long-time memory effects are reflected in a non-exponential decay of the intermediate scattering functions which can be directly observed by neutron spin echo spectroscopy.[16] On much longer time scales a non-exponential relaxation dynamics of proteins has been observed by the single molecule FCS experiments mentioned above.[1,17] Here the internal protein dynamics has been described by fractional Brownian dynamics (FBD), more precisely by a fractional Ornstein–Uhlenbeck (OU) process. The mathematical concept of FBD has been introduced a long time ago by Mandelbrot and Ness[18] in order to model non-Markovian stochastic processes with long-time memory effects. It has been used since then to model such different phenomena as water levels in reservoirs and the time evolution of stock markets. In the context of protein dynamics the model of FBD has been used first to describe the kinetics of oxygen rebinding upon laser flash photolysis.[19] Over the recent years the concept of FBD has stimulated the derivation of generalised Fokker–Planck equations which describe non-Markovian diffusion processes with long time memory in presence of external forces.[20–25]

The concept of fractional Fokker–Planck equations (FFPE) is an interesting route to extend the simple oscillator model for the flexibility of proteins in order to describe QENS from internal protein motions and to bridge the gap to spectroscopic experiments which are sensitive to much longer time scales. The motivation of this paper is to give a short overview of FFPEs, to show how the theory can be used to derive analytical models for QENS from proteins, and to give evidence for fractional Brownian dynamics in proteins by appropriate analyses of molecular dynamics simulations.

## II. Fractional Fokker–Planck equation

### A. Generic form

The Fokker–Planck equation (FPE) is one of the fundamental equations in nonequilibrium statistical mechanics.[26–28] It

† Presented at the 7th International Conference on Quasi-elastic Neutron Scattering, Arcachon, France, September 1–4, 2004.
‡ Affiliated with the University of Orléans.

DOI: 10.1039/b502040a

describes the time evolution of the transition probability density for a Markovian stochastic process, assuming that small increments in time lead to small increments in the stochastic variable under consideration. From a physical point of view Fokker–Planck equations describe diffusion processes in the presence of systematic forces. For Fokker–Planck operators with a discrete spectrum of eigenvalues the Markovian hypothesis leads to solutions and associated correlation functions which exhibit a multiexponential decay in time, with a well defined slowest relaxation mode. In order to generate correlation functions with algebraic long-time tails, as they are often observed in relaxation processes of complex systems, the fractional Fokker–Planck equation (FFPE) has been introduced more recently.[20–23] It is effectively a phenomenological generalisation of the Fokker–Planck equation which leads by construction to non-exponentially decaying solutions. Assuming that $\Omega$ is the stochastic variable under consideration, the fractional Fokker–Planck equation reads

$$\frac{\partial P(\Omega,t)}{\partial t} = \tilde{\tau}^{1-\alpha}\,{}_0\mathscr{D}_t^{1-\alpha}\mathscr{L}_{\rm FP}P(\Omega,t). \tag{2.1}$$

Here $P(\Omega,t) \equiv P(\Omega,t|\Omega_0,t_0)$ is the transition probability density for a move from $\Omega_0$ at time $t_0$ to $\Omega$ at time $t$, and $\mathscr{L}_{\rm FP}$ is the standard Fokker–Planck operator

$$\mathscr{L}_{\rm FP} = -\frac{\partial}{\partial\Omega}a_1(\Omega) + \frac{1}{2}\frac{\partial^2}{\partial\Omega^2}a_2(\Omega), \tag{2.2}$$

where $a_1(\Omega)$ and $a_2(\Omega)$ are, respectively, the drift and fluctuation coefficients which depend in general on $\Omega$. The symbol ${}_0\mathscr{D}_t^{1-\alpha}$ denotes the Riemann–Liouville operator for a fractional derivative of order $1-\alpha$.[29] For an arbitrary function $f$ the latter is defined as

$${}_0\mathscr{D}_t^{1-\alpha}f(t) = \frac{\mathrm{d}}{\mathrm{d}t}\int_0^t \mathrm{d}\tau\,\frac{(t-\tau)^{\alpha-1}}{\Gamma(\alpha)}f(\tau). \tag{2.3}$$

Here $\Gamma(\cdot)$ is the gamma function.[30] In general, a fractional derivative of order $\beta > 0$ is a normal derivative of order $n$, with $n$ being the smallest integer number $\geq \beta$, which is preceded by a fractional integration of order $n-\beta$. The scaling factor $\tilde{\tau}$ ($\tilde{\tau} > 0$) in (2.1) has been introduced to ensure the correct dimension of the right-hand side. The FFPE (2.1) is to be solved with the initial condition $P(\Omega, 0) = \delta(\Omega - \Omega_0)$. One recognises that the standard FPE equation is retrieved in the limit $\alpha \to 1$.

### B. General form of the solution

The construction of the FFPE (2.1) is most easily understood by looking at its Laplace transform, which is defined as $\hat{f}(s) = \int_0^\infty \mathrm{d}t\,\exp(-st)f(t)$ for an arbitrary function $f(t)$ ($\Re s\} > 0$). Performing first an integration of both sides of the FFPE from 0 to $t$ yields

$$P(t,\Omega) - P(\Omega,0) = \tilde{\tau}^{1-\alpha}\int_0^t \mathrm{d}\tau\,\frac{(t-\tau)^{\alpha-1}}{\Gamma(\alpha)}\mathscr{L}_{\rm FP}P(\Omega,\tau),$$

and a subsequent Laplace transform leads to

$$\hat{P}(s,\Omega) - \frac{P(\Omega,0)}{s} = \tilde{\tau}^{1-\alpha}s^{-\alpha}\mathscr{L}_{\rm FP}P(\Omega,\tau).$$

Using that $P(\Omega,0) = \delta(\Omega - \Omega_0)$ one obtains thus

$$\hat{P}(\Omega,s) = \frac{1}{s - [s\tilde{\tau}]^{1-\alpha}\mathscr{L}_{\rm FP}}\delta(\Omega-\Omega_0). \tag{2.4}$$

We assume now that $\mathscr{L}_{\rm FP}$ has a discrete spectrum of eigenvalues. The Dirac distribution may then be expressed in terms of the biorthogonal set of right and left eigenfunctions of $\mathscr{L}_{\rm FP}$, which are defined by the relations[26,28]

$$\mathscr{L}_{\rm FP}P_n(\Omega) = -\lambda_n P_n(\Omega), \tag{2.5}$$

$$\mathscr{L}_{\rm FP}^{+}Q_n(\Omega) = -\lambda_n Q_n(\Omega), \tag{2.6}$$

respectively, and fulfil $(P_n,Q_k) = \delta_{nk}$, where $\delta_{nk}$ is the Kronecker delta. The operator $\mathscr{L}_{\rm FP}^{+}$ is adjoint to $\mathscr{L}_{\rm FP}$, such that $(g,\ \mathscr{L}_{\rm FP}f) = (\mathscr{L}_{\rm FP}^{+}g,f)$, and one has $P_n(\Omega) = Q_n(\Omega)P_{\rm eq}(\Omega)$. The scalar product of two functions $f$ and $g$ is here defined as $(f,\,g) = \int_{-\infty}^{+\infty}\mathrm{d}\Omega\,f(\Omega)g(\Omega)$. Inserting the representation

$$\delta(\Omega-\Omega_0) = \sum_n P_n(\Omega)Q_n(\Omega_0). \tag{2.7}$$

into expression (2.4) yields thus

$$\hat{P}(\Omega,s) = \sum_n \frac{1}{s + (s\tilde{\tau})^{1-\alpha}\lambda_n}P_n(\Omega)Q_n(\Omega_0). \tag{2.8}$$

One can now make use of the relation

$$E_\alpha(-t^\alpha) = \frac{1}{2\pi\mathrm{i}}\oint_{\rm C}\mathrm{d}s\,\frac{\exp(st)}{s(1+s^{-\alpha})}, \tag{2.9}$$

where $E_\alpha(z)$ is the Mittag–Leffler function[31]

$$E_\alpha(z) = \sum_{k=0}^{\infty}\frac{z^k}{\Gamma(1+\alpha k)}. \tag{2.10}$$

The above series expansion shows that $E_\alpha(z)$ is a generalised exponential function, where the gamma function $\Gamma(1+\alpha k)$ replaces the factorial $k!$ in the series representation of a normal exponential function. Therefore the functions $E_\alpha(-t^\alpha)$ may be considered as generalised stretched exponential functions. Using the above relations and the rescaled eigenvalues

$$\lambda_{\alpha,n} := \tilde{\tau}^{1-\alpha}\lambda_n, \tag{2.11}$$

the inverse Laplace transform of eqn. (2.8) can be cast into the form

$$P(\Omega,t) = \sum_n P_n(\Omega)Q_n(\Omega_0)E_\alpha(-\lambda_{\alpha,n}t^\alpha). \tag{2.12}$$

The generalised stretched exponential functions decay monotonically to zero with $t \to \infty$, and for large times one can make the approximation

$$E_\alpha(-\lambda_{\alpha,n}t^\alpha) \approx \frac{\lambda_{n,\alpha}^{-1}t^{-\alpha}}{\Gamma(1-\alpha)}. \tag{2.13}$$

The solution of a FFPE has thus by construction an algebraic long-time tail. In the limit $\alpha \to 1$ each generalised stretched exponential in eqn. (2.12) is replaced by $\exp(-\lambda_n t)$, and one retrieves the eigenfunction representation for the solution of a Fokker–Planck equation.[28] The transition from a FPE to its fractional counterpart leads thus to the replacement of $\exp(-\lambda_n t) \to E_\alpha(-\lambda_{\alpha,n}t^\alpha)$ in the eigenfunction expansion of the general solution.

A remark concerning the equilibrium density is in place here. If the Fokker–Planck operator describes a system close to thermal equilibrium, it possesses only negative eigenvalues, except for one which is zero and which is associated to the eigenfunctions $P_0(\Omega) = P_{\rm eq}(\Omega)$, representing the equilibrium density. The corresponding left eigenfunction is given by $Q_0(\Omega) = 1$. Ordering the (negative) eigenvalues $\lambda_n$ such that $\lambda_0 < \lambda_1 < \lambda_2 \ldots$, where $\lambda_0 = 0$, it follows from the proportionality relation eqn. (2.11) that also $\lambda_{\alpha,0} < \lambda_{\alpha,1}, < \lambda_{\alpha,2} \ldots$, and in particular $\lambda_{\alpha,0} = \lambda_0 = 0$. This shows that the equilibrium solution of a FFPE is the same as the one of the corresponding standard FPE,

$$P_{\rm eq}(\Omega) = \lim_{t\to\infty}P(\Omega,t) = P_0(\Omega). \tag{2.14}$$

It should also be emphasised that a discrete eigenvalue spectrum of a Fokker–Planck operator leads to a strict maximum relaxation time

$$\tau_{\max} = \lambda_1^{-1} \tag{2.15}$$

in the case of normal Brownian dynamics.

### C. Correlation function and its Fourier spectrum

From the general form, eqn. (2.12), of the solution of a FFPE one can derive a formula for the correlation function $c_{\Omega\Omega}(t) := \langle \Omega(t)\Omega(0)\rangle$. Using the relation between the $P_n(\Omega)$ and $Q_n(\Omega)$ and one obtains

$$\begin{aligned} c_{\Omega\Omega}(t) &= \int\int \mathrm{d}\Omega_0\,\mathrm{d}\Omega\,\Omega\Omega_0 P(\Omega,t|\Omega_0,0)P_{\mathrm{eq}}(\Omega_0) \\ &= \sum_{n=1}^{\infty}\left(\int \mathrm{d}\Omega\Omega P_n(\Omega)\right)^2 E_\alpha(-\lambda_{\alpha,n}t^\alpha). \end{aligned} \tag{2.16}$$

It should be noted that the sum in eqn. (2.16) starts with $n = 1$ since there is no net drift in the equilibrium state, and therefore $\int \mathrm{d}\Omega\ \Omega P_0(\Omega) = 0$.

In experiments one measures often the Fourier spectrum of a time correlation function and not the time correlation function itself. The generalised stretched exponential functions introduced in eqn. (2.9) have the convenient feature that they possess an analytical Fourier transform.[32] Defining $\tilde{c}_{\Omega\Omega}(\omega) = \int_{-\infty}^{+\infty} \mathrm{d}t\ \exp(-\mathrm{i}\omega t)c_{\Omega\Omega}(t)$, one obtains

$$\tilde{c}_{\Omega\Omega}(\omega) = \sum_{n=1}^{\infty}\left(\int \mathrm{d}\Omega\,\Omega P_n(\Omega)\right)^2 L_\alpha(\omega;\tau_{\alpha,n}), \tag{2.17}$$

where $L_\alpha(\omega;\tau)$ is the generalised Lorentzian (here $\tau_{\alpha,n} \equiv \tau$ for brevity)

$$L_\alpha(\omega;\tau) = \frac{2\tau\sin(\alpha\pi/2)}{|\omega\tau|(|\omega\tau|^\alpha + 2\cos(\alpha\pi/2) + |\omega\tau|^{-\alpha})}, \quad 0<\alpha\leq 1. \tag{2.18}$$

The relaxation times $\tau_{\alpha,n}$ are given by

$$\tau_{\alpha,n} = \lambda_{\alpha,n}{}^{-(1/\alpha)}, \qquad n \neq 0, \tag{2.19}$$

where $\lambda_{\alpha,n}$ are the rescaled eigenvalues which have been defined in eqn. (2.11) and which appear in definition (2.16) of the correlation function. It is important to note that $L_\alpha(\omega;\tau)$ is singular at $\omega = 0$ if $\alpha \neq 1$. This is due to the fact that $E_\alpha(-(t/\tau)^\alpha)$ is a self-similar function which has no characteristic time scale. The limiting behaviour for large frequencies,

$$L_\alpha(\omega;\tau) \propto \omega^{-(1+\alpha)}, \tag{2.20}$$

differs from that of a Lorentzian, $L(\omega,\tau) = 2\tau/(1 + [\omega\tau]^2)$, which decays as $\propto\omega^{-2}$.

## III. A simple model for QENS from proteins

In the following it will be shown how a FFPE approach can be used to construct a simple model for internal protein dynamics, as it is observed by quasielastic neutron scattering. Two essential features must be taken into account in this case:

(a) The model must describe diffusive motions which are confined in space.

(b) The resulting correlation functions must exhibit long-time memory effects leading to a non-exponential decay in time.

Such a model is the fractional Ornstein–Uhlenbeck process which describes non-Markovian diffusion of a Brownian particle in a harmonic potential. As already mentioned, this model has been recently used to model spectra from fluorescence photon correlation spectroscopy.[17] In contrast to the model by Volino and Dianoux,[15] the confinement of the atomic motions is not modelled by a boundary condition, but by a quadratic potential

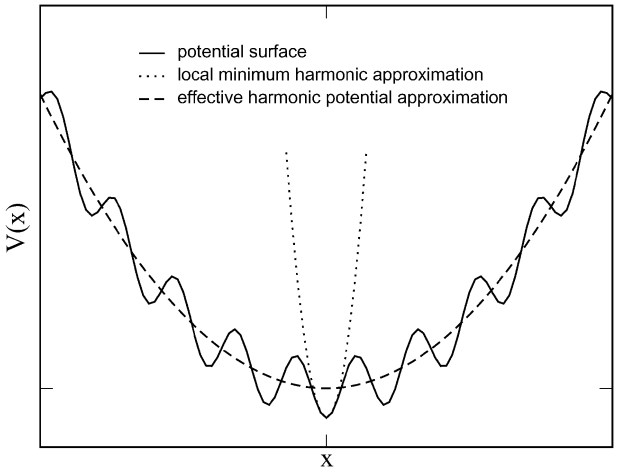


**Fig. 1** Sketch of the potential energy surface of a protein.

$$V(x) = \frac{K}{2}x^2. \tag{3.21}$$

Here $K > 0$ is the force constant of the elastic force $F(x) = -Kx$ which tends to restore the equilibrium position $x = 0$ of the Brownian particle. The latter is a tagged, ''representative atom'' which describes the motion of all atoms in a protein. The potential (3.21) must be interpreted as an *effective* potential, which represents the envelope of a rugged multiminima potential energy surface,[33] as it is shown in Fig. 1. At low temperatures the tagged atom is trapped in one of the local minima and performs harmonic vibrations. If the temperature is raised above the transition temperature $T_g$ of about 200 K, the tagged atom can easily escape the local minima and performs diffusive motions in the effective envelope potential. To account for long-time memory effects, which are characteristic for relaxation processes in complex systems, the motion of the tagged atom is not described by the standard Ornstein–Uhlenbeck process, but by its fractional counterpart. The force constant $K$ describes effectively the softness or ''resilience'' of the protein, which suffices to obtain a qualitative description of elastic neutron scattering from proteins.[9]

### A. Fractional Fokker–Planck equation and its solution

In the following $\Omega \to x$ describes the position of a Brownian particle, which diffuses in the harmonic potential (3.21). In this case the drift coefficient in the Fokker–Planck operator (2.2) is set to $a_1(x) = -\eta x$ and the fluctuation coefficient to $a_2(x) = 2D$, where $\eta$ is an inverse relaxation time and $D$ is the short time diffusion coefficient. The Ornstein–Uhlenbeck process has been extensively studied in the past, and the left and right eigenfunctions of the corresponding Fokker–Planck operator

$$\mathscr{L}_{\mathrm{FP}} = \eta\frac{\partial}{\partial x}x + D\frac{\partial^2}{\partial x^2} \tag{3.22}$$

are well known.[26,28] One obtains

$$Q_n(x) = \frac{1}{\sqrt{2^n n!}}H_n(x\sqrt{\eta/2D}) \tag{3.23}$$

for the left eigenfunctions corresponding to the negative eigenvalues

$$\lambda_n = n\eta,\ n = 0,1,2,\ldots \tag{3.24}$$

Here $H_n(\cdot)$ is the $n$th Hermite polynomial.[30] As outlined above, the right eigenfunctions are given by $P_n(x) = P_{\mathrm{eq}}(x)Q_n(x)$, where $P_{\mathrm{eq}}(x) = P_0(x)$ is the equilibrium density.

The latter reads here

$$P_{\mathrm{eq}}(x) = \sqrt{\frac{\eta}{2\pi D}} \exp\left(-\frac{\eta x^2}{2D}\right). \tag{3.25}$$

Since the equilibrium density must be proportional to the Boltzmann factor, $P_{\mathrm{eq}}(x) \propto \exp(-\beta V(x))$, it follows from eqn. (3.25) that

$$\frac{D}{\eta} = \frac{k_{\mathrm{B}}T}{K}. \tag{3.26}$$

Here $\beta = 1/k_{\mathrm{B}}T$ is the inverse temperature divided by the Boltzmann constant $k_{\mathrm{B}}$ and $K$ is the force constant of the quadratic potential in eqn. (3.21). Defining the scaled positions

$$x' = \frac{x}{\sqrt{\langle x^2 \rangle}} \tag{3.27}$$

where $\langle x^2 \rangle$ is the mean square position fluctuation

$$\langle x^2 \rangle = \frac{k_{\mathrm{B}}T}{K} \tag{3.28}$$

and the scaled relaxation constant

$$\eta_\alpha = \tilde{\tau}^{1-\alpha}\eta, \tag{3.29}$$

one obtains from eqn. (2.12)[20,23]

$$P(x', t) = \frac{\exp(-x'^2/2)}{\sqrt{2\pi}} \sum_{n=0}^{\infty} \frac{1}{2^n n!} H_n\left(\frac{x'}{\sqrt{2}}\right) H_n\left(\frac{x'_0}{\sqrt{2}}\right) E_\alpha(-n\eta_\alpha t^\alpha). \tag{3.30}$$

Here $E_\alpha(\cdot)$ is the Mittag–Leffler function defined in eqn. (2.10).

### B. The autocorrelation function and its memory function

The autocorrelation function of the scaled variable $x'$ is obtained from the general expression (2.16), using that here $\Omega \to x'$ and $\int \mathrm{d}x'\, x' P_n(x') = \delta_{n,1}$. Defining the normalized autocorrelation function $\psi(t) \equiv c_{x'x'}(t)$, one obtains

$$\psi(t) = E_\alpha(-\eta_\alpha t^\alpha). \tag{3.31}$$

In the limit $\alpha \to 1$ the exponentially decaying correlation function of the standard Ornstein–Uhlenbeck process is retrieved. Fig. 2 shows $\psi$ as given by eqn. (3.31) for $\alpha = 1/2$ (solid line), its limit for $\alpha \to 1$ (dashed line), and for comparison also the "normal" stretched exponential $\exp(-[t/\tau]^\alpha)$ with $\alpha = 1/2$. The latter is also known as Kohlrausch–Williams–Watt (KWW) function and has been used extensively to model dielectric relaxation processes.[34] For identical parameters $\tau$ and $\alpha$ it decays more rapidly with time than the correlation function, eqn. (3.31), but still slower than an exponential

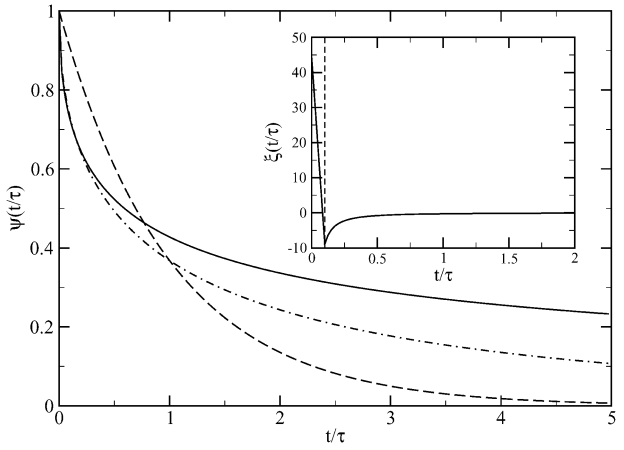


**Fig. 2** Model correlation function for the fractional OU process with $\alpha = 1/2$ (solid line), the exponential $\exp(-[t/\tau])$ (dashed line), and the stretched exponential $\exp(-[t/\tau]^\alpha)$ for $\alpha = 1/2$ (dashed–dotted line).

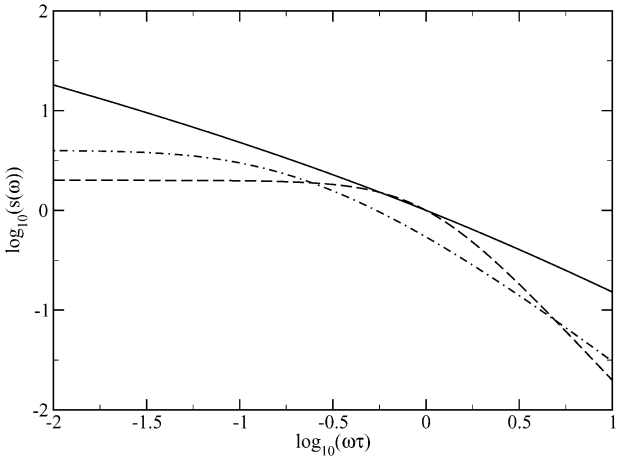


**Fig. 3** The Fourier spectra corresponding to the model correlation functions depicted in Fig. 2.

function. The inset shows the memory function of $\psi(t)$ which is discussed below. It is worthwhile noting that the correlation function of the fractional Ornstein–Uhlenbeck process has the analytical form $\psi(t) = \exp([t/\tau])\mathrm{erfc}([t/\tau]^{1/2})$ if $\alpha = 1/2$.[31]

The Fourier spectrum of $\psi(t)$ is a single generalised Lorentzian,

$$\tilde{\psi}(\omega) = \frac{2\tau_\alpha \sin(\alpha\pi/2)}{|\omega\tau_\alpha|(|\omega\tau_\alpha|^\alpha + 2\cos(\alpha\pi/2) + |\omega\tau_\alpha|^{-\alpha})}, 0 < \alpha \leq 1, \tag{3.32}$$

where $\tau_\alpha$ is given by

$$\tau_\alpha = {\eta_\alpha}^{-1/\alpha} \tag{3.33}$$

Fig. 3 shows the Fourier transforms of the correlation functions depicted in Fig. 2. The spectrum corresponding to a fractional Ornstein–Uhlenbeck process is almost featureless. It reflects that the memory function has no characteristic time scale and is self-similar in the sense of a fractal on the frequency axis: any zoom on the spectrum yields a similar pattern. The KWW model does in general not lead to an analytical form for the Fourier transform of the associated time correlation function. An exception is the case $\alpha = 1/2$, which is depicted in Fig. 3. For practical applications the Fourier transform of the KWW model may be approximated by algebraic functions.[35]

The non-exponential decay of $\psi(t)$ can be quantified by using the concept of memory functions, which have been introduced by Zwanzig.[36] In the full Hamiltonian description of a many body system the autocorrelation function $\psi(t)$ of any phase space variable fulfils a Volterra-type equation of the form

$$\frac{\mathrm{d}}{\mathrm{d}t}\psi(t) = -\int_0^t \mathrm{d}\tau\, \xi(t-\tau)\psi(\tau), \tag{3.34}$$

where the kernel $\xi(\cdot)$ is the memory function associated with $\psi(t)$. The latter can be formally expressed in terms of all phase space variables. One sees easily that an exponential decay of $\psi(t)$ can be produced by a memoryless process where $\xi(t) = (1/\tau)\delta(t)$. In this case eqn. (3.34) becomes a simple differential equation, with $\psi(t) = \exp(-t/\tau)$ as solution. A comprehensive introduction into the theory of memory functions can be found in the monograph by Boon and Yip.[37] Here it matters only that relation (3.34) is *exact* and that any physical model for a correlation function is thus essentially a model for the memory function. In this context it is important to note that the commonly used Kohlrausch–Williams–Watt model, in which the correlation function is described as stretched exponential, $\psi(t) = \exp(-[t/\tau]^\alpha)$ $(0 < \alpha \leq 1)$, has no associated memory function. From a statistical mechanics point of view it does thus not belong to the class of "admissible" models.[32]

 

As the position of a Brownian particle is one of the variables spanning the phase space of the solute particle itself and the surrounding solvent, its autocorrelation function should verify a memory function equation of the form (3.34). The memory function associated with a fractional Ornstein–Uhlenbeck process has been recently derived in ref. 32, using the Laplace transform of the memory function eqn. (3.34). The latter can be derived from relation (2.9), the rhs of which can be interpreted as an inverse Laplace transform. We skip the mathematical subtleties which are discussed in ref. 32 and give directly the result. For any time $t > 0$ the memory function has the form

$$\xi(t) = \frac{\alpha - 1}{\Gamma(\alpha)\tau_\alpha^2}\left(\frac{t}{\tau_\alpha}\right)^{\alpha-2}, \quad t>0, \tag{3.35}$$

for $0 < \alpha < 1$ and fulfils at the same time

$$\int_0^\infty \mathrm{d}t\ \xi(t) = 0. \tag{3.36}$$

As discussed in ref. 32, $\xi(t)$ is a distribution. For any $\varepsilon > 0$ it may be represented by a normal function which has the form (3.35) for $t \geq \varepsilon$, and by an expression of the form $\xi(t) = A + Bt$ for $0 \leq t < \varepsilon$. In the limit $\varepsilon \to 0^+$ the form of $\xi(t)$ for $t \in [0,\varepsilon)$ does not matter, as long as eqn. (3.36) is fulfilled and $\xi(t)$ is continuous. Property (3.35) indicates long time memory effects through an algebraic decay of the memory function and property (3.36) the absence of a characteristic time scale. The latter is defined through $\tau^{-1} = \int_0^\infty \mathrm{d}t\ \xi(t)$, as in the case of memoryless Brownian motion.

### C. Mean-square displacement

For small times the non-exponential decay of $\psi(t)$ leads to a "subdiffusive" increase of the mean square displacement (MSD), instead of an increase $\propto t$, which is characteristic for Einstein diffusion. We note first that the MSD is given by (here the unscaled variable $x$ is used)

$$W_{xx}(t) = \langle [x(t) - x(0)]^2 \rangle = 2\langle x^2 \rangle\ (1 - \psi(t)) \tag{3.37}$$

for motions which are confined in space, where $\langle x^2 \rangle < \infty$. Relation (3.31) shows that

$$W_{xx}(t) = 2\langle x^2 \rangle\ (1 - E_\alpha(-\eta_\alpha t^\alpha)) \tag{3.38}$$

for a fractional Ornstein–Uhlenbeck process. Using this result shows that for small times

$$W(t) \approx 2D_\alpha t^\alpha \tag{3.39}$$

where $D_\alpha = \tilde{\tau}^{1-\alpha} D/\Gamma(1 + \alpha)$ and $D = k_\mathrm{B}T\eta/K$ is the normal short time diffusion constant. For the standard Ornstein–Uhlenbeck process one finds, in contrast, that the mean square displacement for small times is given by $W(t) \approx 2Dt$, which corresponds to Einstein diffusion.

### D. Dynamic structure factor

The fundamental quantity measured in neutron scattering experiments is the dynamic structure factor, $S(q, \omega)$. Here $q$ and $\omega$ are, respectively, the momentum and energy transfer from the neutron to the sample in units of $\hbar$. Formally the dynamic structure factor can be written as,

$$S(q,\omega) = \frac{1}{2\pi}\int_{-\infty}^{+\infty} \mathrm{d}t \exp(-i\omega t) I(q,t), \tag{3.40}$$

where $I(q,t)$ is the intermediate scattering function. For the moment it will be assumed that the scattering system can be described by a single representative atom which moves under the influence of isotropic forces and whose dynamics is described by a FFPE. Since the intermediate scattering function is a time correlation function,[38,39] one writes by analogy with eqn. (2.16)

$$\begin{aligned} I(q,t) &= \int\int \mathrm{d}x_0\, \mathrm{d}x\ \exp(\mathrm{i}q[x - x_0]) P(x,t|x_0,0) P_\mathrm{eq}(x_0) \\ &= \sum_{n=0}^{\infty} \left| \int \mathrm{d}x\ \exp(\mathrm{i}qx) P_n(x) \right|^2 E_\alpha(-\lambda_{\alpha,n} t^\alpha). \end{aligned} \tag{3.41}$$

In contrast to eqn. (2.16) the sum in eqn. (3.41) runs from 0 to $\infty$, since the term with $n = 0$ does not vanish here. This term yields in effect the elastic incoherent structure factor (EISF), which is defined as the limit of $I(q,t)$ for $t \to \infty$,

$$\mathrm{EISF}(q) = \left| \int \mathrm{d}x \exp(\mathrm{i}qx) P_0(x) \right|^2. \tag{3.42}$$

Inserting expression (3.41) into the definition (3.40) of the dynamic structure factor, one recognises easily that the term corresponding to $n = 0$ yields a contribution of the form $\mathrm{EISF}(q)\delta(\omega)$ and gives thus rise to elastic scattering. Moreover the EISF is the same for the FFPE and its non-fractional counterpart.

If the dynamical model is the fractional Ornstein–Uhlenbeck process, the intermediate scattering function takes the form

$$I(q,t) = \exp(-q^2\langle x^2 \rangle) \sum_{n=0}^{\infty} \frac{q^{2n}\langle x^2 \rangle^n}{n!} E_\alpha(-n\eta_\alpha t^\alpha). \tag{3.43}$$

In the limit $\alpha \to 1$ the generalised stretched exponential functions become normal exponential functions, $E_\alpha(-n\eta_\alpha t^\alpha) \to \exp(-n\eta t)$. Since $\exp(-n\eta t) = \exp(-\eta t)^n$, the series in eqn. (3.43) represents the function $\exp(q^2\langle x^2 \rangle \exp[-\eta t])$ in this case, and one retrieves the intermediate scattering function corresponding to the standard OU process,

$$\lim_{\alpha \to 1} I(q,t) = \exp(-q^2\langle x^2 \rangle (1 - \exp[-\eta t])). \tag{3.44}$$

In the general case, where $0 < \alpha < 1$, a closed form such as eqn. (3.44) cannot be given, since $E_\alpha(-n\eta_\alpha t^\alpha) \neq E_\alpha(-\eta_\alpha t^\alpha)^n$. The values of the intermediate scattering function for $t = 0$ and $t \to \infty$ do, however, not depend on $\alpha$. Since $E_\alpha(0) = 1$ it follows that $I(q,\ 0) = 1$, and for $t \to \infty$ one obtains the EISF,

$$\mathrm{EISF}(q) = \exp(-q^2\langle x^2 \rangle). \tag{3.45}$$

The dynamic structure factor is obtained by the Fourier transform eqn. (3.40), inserting expression (3.43):

$$S(q,\omega) = \exp(-q^2\langle x^2 \rangle) \left\{ \delta(\omega) + \sum_{n=1}^{\infty} \frac{q^{2n}\langle x^2 \rangle^n}{n!} \frac{1}{2\pi} L_\alpha(\omega; \tau_{\alpha,n}) \right\}. \tag{3.46}$$

The generalized Lorentzians $L_\alpha(\omega;\tau)$ are given by eqn. (2.18). Combining eqns. (2.11), (2.19) and (3.24) one finds that the relaxation rates are given by

$$\tau_{\alpha,n} = \frac{\tilde{\tau}}{(n\eta\tilde{\tau})^{1/\alpha}}. \tag{3.47}$$

In the limit $\alpha \to 1$ an analytical expression does not only exist for the intermediate scattering function, but also for the dynamic structure factor. As outlined in the Appendix, one finds that

$$\lim_{\alpha \to 1} S(q,\omega) = \mathrm{EISF}(q) \left\{ \delta(\omega) + \frac{1}{\eta} \chi\left( q^2\langle u^2 \rangle, \frac{\omega}{\eta} \right) \right\}, \tag{3.48}$$

where $\chi(\cdot\,,\cdot)$ is given by

$$\chi(a,\omega) = \tfrac{1}{\pi} \mathscr{R}\{(-a)^{-\mathrm{i}\omega} \gamma(\mathrm{i}\omega, -a)\}, \quad \omega \neq 0. \tag{3.49}$$

As usual, $\gamma(\cdot\,,\cdot)$ denotes the incomplete gamma function.[30]

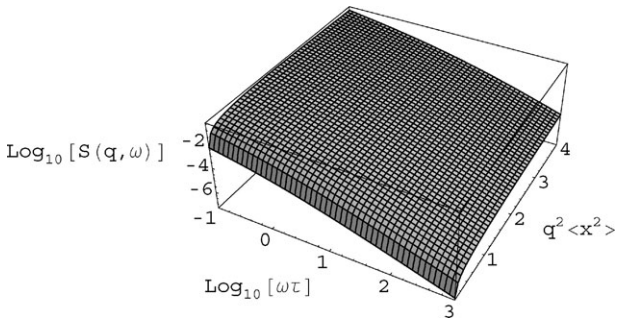


**Fig. 4** Dynamic structure factor corresponding to a fractional OU process. The $\omega$-axis and the ordinate are on a logarithmic scale. The smallest value for $q^2\langle x^2\rangle$ is 0.01.

Figs. 4 and 5 show, respectively, the dynamic structure factor for the fractional OU process ($\alpha = 0.5$) and its standard counterpart. The fractional OU process leads to an almost featureless form of $S(q, \omega)$. Here 20 terms in the series (3.46) have been taken into account, checking empirically the convergence in the given $q$-range. The fact that QENS spectra from hydrated protein powders depend very little on $q$ has been observed by many experimentalists and makes possible to average the experimental spectra over several detectors, in order to obtain a better statistics. In case of normal Brownian dynamics the dynamic structure factor has a finite width, which is well visible in Fig. 5 and which is separately given in Fig. 6. For large $q$-values the $Dq^2$-law of free diffusion is recovered, as for the model of diffusion in a spherical cavity.[15]

### E. An application to QENS reference data

In the following we discuss the application of the fractional OU process as a model for QENS caused by internal motions in myoglobin. For this purpose the data from Doster *et al.* are used,[3] which have been obtained from $D_2O$-hydrated myoglobin powders. The use of hydrated protein powders has been quite popular in the past, since global protein motions need not be considered for such a system. To cover a large energy transfer range the data have been combined from measurements with two different spectrometers at the Institut Laue-Langevin in Grenoble. The spectra for energy transfers $\Delta E <$ 0.1 meV have been obtained with the backscattering spectrometer IN13 and those for $\Delta E > 0.1$ meV with the time-of-flight spectrometer IN6. The respective energy resolutions (HWHM) are $\delta E = 8$ μeV and $\delta E = 50$ μeV.

If the fractional Ornstein–Uhlenbeck process is used as a model for experimental experimental QENS data, one works effectively with 3 free parameters, which are (a) the parameter $\alpha$, (b) the relaxation constant $\tau_{\alpha,1}$ defined by relation (3.47), and (c) the mean square fluctuation $\langle x^2\rangle$. With increasing order $n$ the relaxation times $\tau_{\alpha,n}$ are obtained through $\tau_{\alpha,n} = n^{-1/\alpha}\tau_{\alpha,1}$. The model spectrum must be fitted to experimental data which

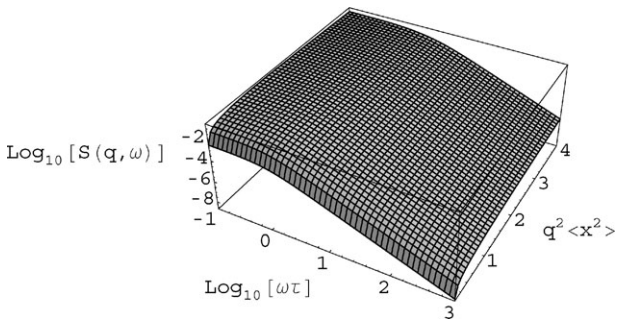


**Fig. 5** For comparison with Fig. 4: Dynamic structure factor corresponding to a standard OU process.

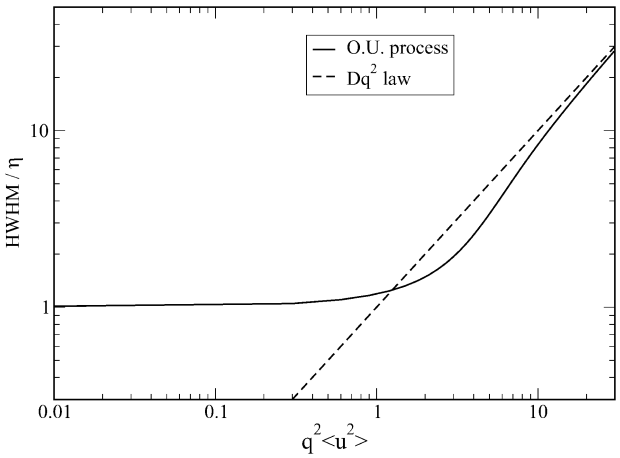


**Fig. 6** HWHM of the QENS spectrum for a standard Ornstein–Uhlenbeck process as a function of $q^2$.

are necessarily obtained in a finite frequency window. The instrumental resolution defines the lower end of this window and for high frequencies mechanical or other physical conditions limit the highest detectable energy of a neutron. Since the experimental spectra are not known outside a certain frequency window they cannot be properly normalized for comparison with the model spectrum, for which $\int_{-\infty}^{+\infty} d\omega\, S(q,\omega) = I(q,0) =$ 1. In addition the model spectrum is singular for $\omega \to 0$ if $\alpha$ is not exactly equal to one. Only in the latter case one obtains a profile with a finite, absolute amplitude to which the data can be adjusted. To match the experimental and the model spectrum, an additional free amplitude parameter must therefore be introduced into the model. The fit of the model spectrum, eqn. (3.46) to the experimental QENS data published in ref. 3, which is shown in Fig. 8, has nevertheless been obtained by using three free parameters, since the parameter $q^2\langle x^2\rangle$ could be fixed by using data from elastic scans and MD simulations. Fig. 7 shows the EISF for myoglobin at 277 K and 320 K obtained from elastic neutron scattering,[3] as compared to molecular dynamics simulation data at 300 K,[40] and a fit of the Gaussian model eqn. (3.45) to the simulation data (solid line and filled circles). The fit was performed in the range $q <$ 20 $nm^{-1}$. This value can be considered as an upper limit for the applicability of FBD models, since such models can certainly not describe very localised motions which are seen for larger $q$-values. FBD models give a *global* view of the internal dynamics of proteins. The fit of the Gaussian EISF (3.45) yields here $\langle x^2\rangle = 1.25 \times 10^{-3}$ $nm^2$. To obtain the appropriate value for $q$

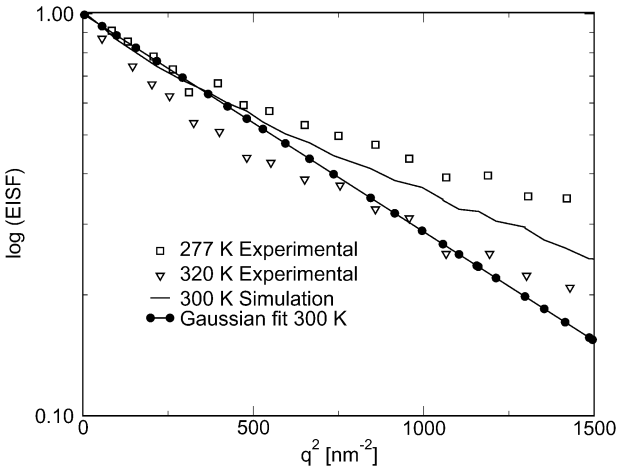


**Fig. 7** Experimental EISF of myoglobin for 277 K (squares), 320 K (triangles) from ref. 3, compared to MD simulation results for 300 K[40] (solid line), and a fit of the Gaussian model in eqn. (3.45) for $q^2 <$ 500 $nm^{-2}$.

 

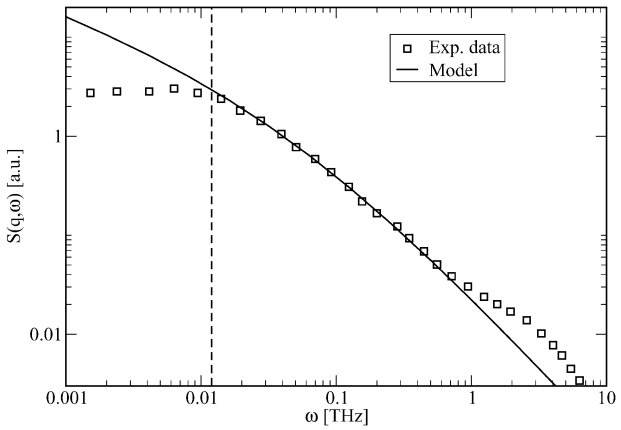


**Fig. 8** Fit of the model in eqn. (3.46) to the experimental QENS data in ref. 3 at 300 K (solid line and squares, respectively). Here the energy transfer is given in THz (angular frequency). Apart from a global amplitude factor, the fitted parameters are $\tau = 24.12$ ps and $\alpha = 0.51$. More explanations are given in the text. The vertical dashed line indicates the resolution of the spectrometer IN13 at the Institut Laue-Langevin in Grenoble, which is 8 μeV $\approx$ 0.012 THz (angular frequency).

the data listed in the above reference for the experiment on IN6 have been used. The incident wavelength was $\lambda_0 = 0.51$ nm, and the scattering angle $\theta = 58.8^\circ$. Approximating $q \approx q_{el} = 2k_0\sin(\theta/2)$, where $q_{el}$ is the elastic momentum transfer, and $k_0 = 2\pi/\lambda_0$ is the wavenumber corresponding to the wavelength of the incident neutrons, one finds $q = 12.04$ nm$^{-1}$ and $q^2\langle x^2\rangle = 0.181$.

The value for $q^2\langle x^2\rangle$ obtained from the EISF can now be used for the fit of the FBD model in eqn. (3.46). Table 1 shows the parameters $\alpha$ and $\tau$ as a function of the number $n_c$ of terms which is considered in eqn. (3.46). For the $n_c = 5$ the series has practically converged. One finds that $\alpha \approx 0.5$ and $\tau \approx 24$ ps. The amplitude factors are not shown here.

Since the fractional Ornstein–Uhlenbeck process is a model which is based on the representation of protein dynamics by an "effective" atom, localised specific motions cannot be described within the model and only low frequencies, describing slow relaxation processes, should be considered. Fig. 8 gives an idea how the experimental data could be extrapolated to frequencies below the resolution limit, which is indicated by the vertical dashed line. The latter refers to the IN13 spectrometer which has been used in the low frequency region. It should be noted that $\omega$ in Fig. 8 is an *angular* frequency.

## IV. Simulation-based modelling of protein dynamics

### A. Motivation for combined neutron scattering and simulation experiments

With the development of computers in the early 1950's simulation methods have become an indispensable tool for theorists and experimentalists, which allow to study condensed matter systems on an intermediate complexity scale between an analytical model and a real system. Since the pioneering work of Rahman on liquid argon,[41] molecular dynamics (MD) simulations have been used in a vast number of applications in solid state physics, physical chemistry, and in biology. A compilation of early papers can be found in ref. 42 and refs. 43 and 44 are classic textbooks on molecular dynamics and Monte Carlo simulations. The combination of neutron scattering experiments and MD simulations is a particularly powerful method to study the structure and dynamics of condensed matter on the atomic scale. Both methods cover the same time and length scales, roughly 1 Å to 100 Å and 1 ps to 10 ns, respectively, and the comparison is very direct since neutrons interact with the atomic nuclei, which are the simulated objects. If recoil effects can be neglected in the scattering experiment[45] and if the dynamics of the scattering system is determined by the laws of classical mechanics, the coherent and the incoherent intermediate scattering functions can be computed from MD simulations *via*

$$I_{coh}(\boldsymbol{q}, t) = \frac{1}{N}\sum_{i,j} b_{i,coh} b_{j,coh} \langle \exp(i\boldsymbol{q}^T \cdot [\boldsymbol{R}_i(t) - \boldsymbol{R}_j(0)])\rangle, \tag{4.50}$$

$$I_{inc}(\boldsymbol{q}, t) = \frac{1}{N}\sum_{i} b_{i,inc}^2 \langle \exp(i\boldsymbol{q}^T \cdot [\boldsymbol{R}_i(t) - \boldsymbol{R}_i(0)])\rangle. \tag{4.51}$$

Here $\boldsymbol{R}_i(t)$ are the trajectories of the $N$ atomic positions and $b_{i,coh}$ and $b_{i,inc}$ are, respectively, the coherent and incoherent scattering lengths of atom $i$.[38,39] The symbol $^T$ denotes a transposition. MD simulations have the enormous advantage that information on the simulated system is available at all description levels, ranging from the trajectory of an individual atom to averages and correlation functions involving the whole simulated system. In the recent past they have been used to interpret neutron scattering experiments from systems ranging from molecular liquids to proteins. A broader overview on combined neutron scattering and simulation studies can be found in ref. 46 and an update will appear soon. In the context of this paper the articles[40,47–49] and the review[50] are of interest.

A simple application in which MD simulations are used to interpret QENS from proteins has been published in ref. 40. The basic question addressed in this article is which type of motion contributes most to the quasielastic scattering spectrum of neutrons from myoglobin at room temperature. The experimental data which have been used in ref. 40 are the same as those used above to fit the FBD model.[3] Figs. 10 and 11 confront the simulation results with the experimental data, using two different trajectories for data analysis: the "raw" MD trajectory, and a trajectory in which internal side-chain motions have been filtered out and only rigid-body motions of the side chains are left. One notices first that the EISF is well estimated by the raw simulation data, which indicates that the atomic fluctuations measured by elastic neutron scattering and those obtained from simulation are very similar. The agreement of the QENS spectra is less good for $\omega > 0.5$ meV, which may be explained by the fact that the experimental spectrum has been modified by subtracting a vibrational background.[3] In any case the agreement is excellent in the safe quasielastic region. The rigid body trajectories have been produced by fitting to each side chain and each time frame a respective reference structure, which was taken to be the initial structure in the MD production run. The simulation results show that elastic and quasielastic neutron scattering from myoglobin (and quite probably from *all* globular proteins) is essentially produced by rigid-body small-step diffusion of whole residues (see Fig. 9). Internal motions on the residue scale do almost not contribute to quasielastic and elastic neutron scattering. This interpretation of the QENS results is very different from the one in ref. 3, where the EISF is fitted by an asymmetric two-site jump model, thus assuming jump diffusion and not a continuous diffusion process.

Most, if not all combined MD and neutron scattering studies of protein dynamics, which have been published so far, have

**Table 1** Parameters for the fit of the fractional Ornstein–Uhlenbeck model shown in Fig. 8

| | $n_c = 1$ | $n_c = 2$ | $n_c = 5$ | $n_c = 10$ |
|---|---|---|---|---|
| $\alpha$ | 0.501 | 0.508 | 0.509 | 0.509 |
| $\tau$/ps | 20.9 | 23.1 | 23.3 | 23.3 |

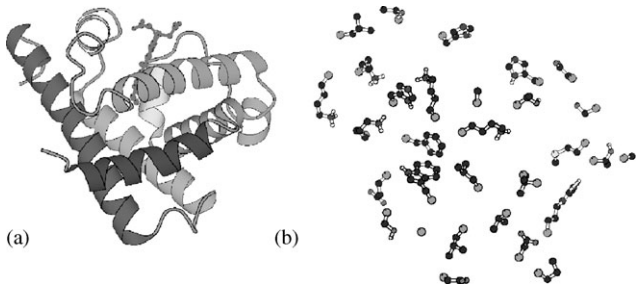


**Fig. 9** Left: protein backbone of myoglobin. Right: 31 selected side chains.

been devoted to investigate relatively fast, "liquid-like" and vibrational motions, as well as the coupling between solvent and protein dynamics. In the following it will be shown that MD simulations can also reveal the presence of very slow relaxation modes, which are *a priori* too slow to be fully seen on the MD/QENS time scale.

### B. Anomalous diffusion

One of the very first analyses of a MD simulation is the calculation of the average mean-square displacement of all or a part of the atoms in the simulated system,

$$W(t) = \frac{1}{N}\sum_{j=1}^{N} w_j \langle [\boldsymbol{R}_j(t) - \boldsymbol{R}_j(0)]^2 \rangle. \qquad (4.52)$$

Here $N$ is the number of atoms under consideration, and $w_j$ are appropriate weights, with $\sum_{j=1}^{N} w_j = N$. Fig. 13 shows the simulated average mean-square displacement of a lysozyme protein in solution at ambient temperature and pressure. The protein is depicted in Fig. 12. The simulation has been performed for one lysozyme protein in a solution of 3403 water molecules in a rectangular box of $6.16 \times 4.19 \times 4.61$ nm$^3$ at ambient temperature and pressure, using the Amber94 potential which includes an adapted TIP3P water model.[51] More details can be found in ref. 52 and will be published elsewhere. The weights in (4.52) have been chosen proportional to the squared incoherent scattering lengths of the 1960 explicit lysozyme atoms, $w_j \propto b_{j,\mathrm{inc}}{}^2$. This weighting scheme corresponds in practise to considering only the hydrogen atoms, since the bound incoherent scattering cross section, $\sigma_{\mathrm{H,inc}} = 4\pi b_{\mathrm{H,inc}}{}^2$, is much larger than all other scattering cross sections.[38,39] It is important to note that global translations and rotations of the lysozyme molecule have been subtracted prior to analysis. In this way only internal protein motions are left. The subtraction of global motions has been achieved by performing for each time frame of the original MD trajectory a rigid-body fit of the lysozyme structure onto the initial structure in the trajectory.[53]

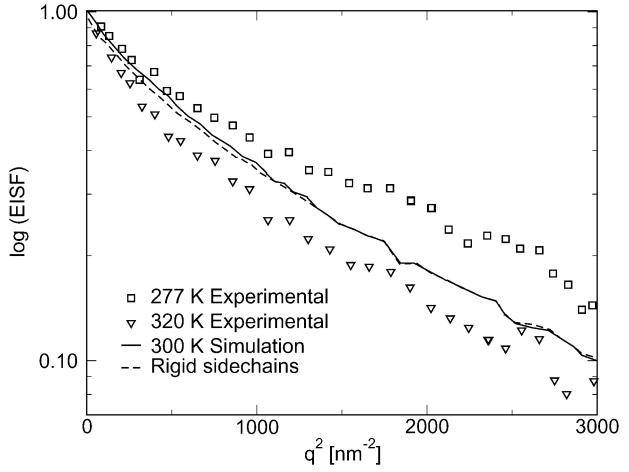


**Fig. 10** EISF of myoglobin from simulation[40] at $T = 300$ K (solid line and dashed line) and experiment[3] (squares = 277 K, triangles = 320 K). The solid line shows the result obtained from straightforward analysis of the MD trajectory and the dashed line has been obtained by filtering out internal motions of the protein side-chains.

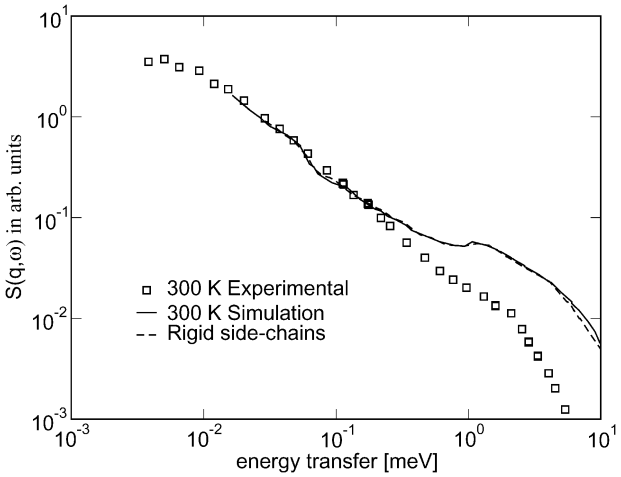


**Fig. 11** Results for the quasielastic spectrum corresponding to Fig. 10, where the experimental data are given for 300 K. In contrast to the simulated spectrum, the experimental spectrum has been modified by subtracting a vibrational background.[3]

The solid line in Fig. 13 shows the neutron-weighted average mean-square displacement of the atoms in lysozyme together with a fit of the FBD model (3.38). Assuming isotropic diffusion, the mean square fluctuation $\langle x^2 \rangle$ is here to be replaced by $\langle \boldsymbol{u}^2 \rangle$, where $\langle \boldsymbol{u}^2 \rangle = \langle x^2 \rangle + \langle y^2 \rangle + \langle z^2 \rangle$ is the position fluctuation in Cartesian coordinates. One writes thus,

$$W(t) = 2\langle \boldsymbol{u}^2 \rangle \, (1 - E_\alpha(-[t/\tau]^\alpha)). \qquad (4.53)$$

where $\tau$ corresponds to the relaxation time scale $\tau_{\alpha,1}$ defined in eqn. (3.47). The fit has been performed for the parameters $\tau$ and $\alpha$ only, providing $\langle \boldsymbol{u}^2 \rangle = 0.019$ nm$^2$ from a separate calculation from the MD trajectory. The resulting parameters are $\tau = 33.5$ ps and $\alpha = 0.49$. These values are remarkebly similar to those found in Table 1 and which correspond to the fit of the QENS data for myoglobin shown in Fig. 8. The inconsistent behaviour of the simulated mean-square displacement with respect to the plateau value $W(\infty) = 2\langle \boldsymbol{u}^2 \rangle$ (horizontal dotted line) is typical for MD simulations and indicates that the simulation is not long enough to establish the convergence of $W(t)$ to the plateau value predicted by the *same*

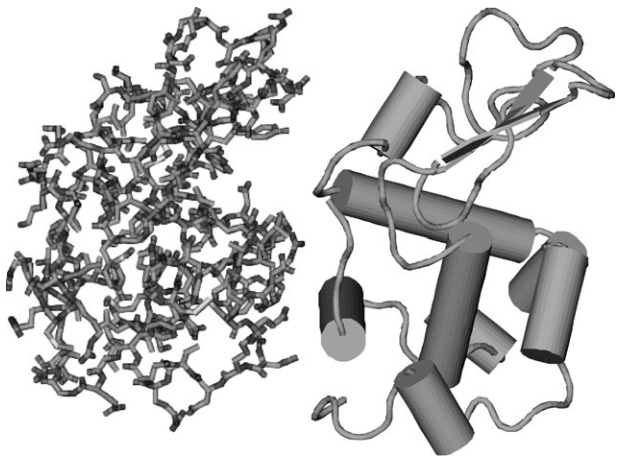

**Fig. 12** A lysozyme molecule represented by its covalent bond structure (left) and a cartoon showing the secondary structure elements (right).

 

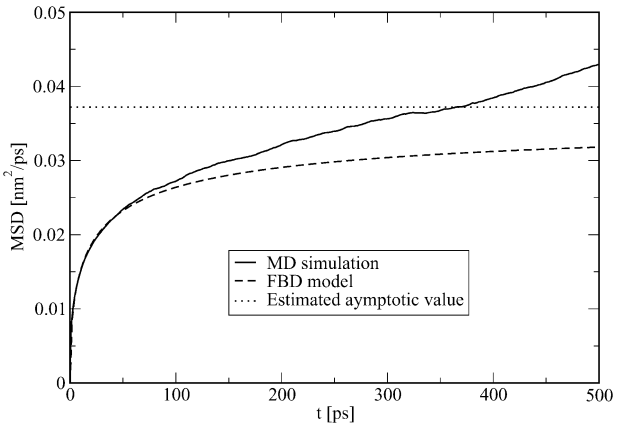


**Fig. 13** Average atomic mean square displacement for lysozyme from MD simulation (solid line), a fit of expression (4.53) which is predicted by a fractional OU process (dashed line), and the asymptotic value which has been obtained by a separate calculation from the MD trajectory (dotted line).

simulation. It must be emphasised that the latter is a purely static quantity and requires less data for the same statistical accuracy than the study of extremely slow relaxation processes. Therefore the average position fluctuation can be obtained with some confidence, although it must be clearly stated that the exact value is not known. In this context it is worthwhile recalling that MD simulation yields position fluctuations which are close to the ones obtained by elastic neutron scattering (see Fig. 10). Using the scaling behaviour of the fractional Ornstein–Uhlenbeck process, one can estimate a typical convergence time of $W(t)$, even if the latter is much longer than the length of the underlying MD trajectory. For this purpose one can make use of approximation (2.13) and write

$$W(t) \approx 2\langle \boldsymbol{u}^2 \rangle \left(1 - \frac{(t/\tau)^{-\alpha}}{\Gamma(1-\alpha)}\right). \tag{4.54}$$

The mean square displacement converges thus very slowly to its plateau value $W(\infty)$. If $t_p$ defines the time where $W(t)$ has attained $p$% of the plateau value, one obtains for $\alpha = 0.5$ a value of $t_p = 127\ \tau$ for $p = 95$ and $t_p = 3183\ \tau$ for $p = 99$. These values must be compared, respectively, to $t_p = 3.00\ \tau$ and $t_p = 4.61\ \tau$ for exponential relaxation. One recognises that normal exponential relaxation is clearly not an appropriate model for internal protein dynamics.

### C. Slow collective relaxation

**1. Memory function for density fluctuations.** So far the internal dynamics of proteins has been discussed in the light of single particle dynamics. Recent MD simulation results show that FBD is also a good model for *collective* relaxation.[32] In the following we take the Fourier-transformed particle density fluctuation of a protein to be the dynamical variable of interest,

$$\begin{aligned}\delta\rho(\boldsymbol{q},t) &= \rho(\boldsymbol{q},t) - \langle \rho(\boldsymbol{q},t)\rangle, \text{with}\, \rho(\boldsymbol{q},t) \\ &= \sum_{j=1}^{N} w_i \exp(\mathrm{i}\boldsymbol{q}\cdot\boldsymbol{R}_j(t)).\end{aligned} \tag{4.55}$$

To be able to make contact with experiment, the weights $w_j$ are chosen to be proportional to the coherent neutron scattering length of atom $j$.[38] With this choice the correlation function associated with $\delta\rho(\mathbf{q}, t)$ is the coherent intermediate scattering function (the asterisk denotes the complex conjugate),

$$c(\boldsymbol{q},t) = \langle \delta\rho^*(\boldsymbol{q},0)\delta\rho(\boldsymbol{q},t)\rangle \tag{4.56}$$

Since $\delta\rho(\boldsymbol{q},t)$ can be interpreted as a dynamical variable in phase space there is a memory function which is associated with its autocorrelation function, such that

$$\frac{\mathrm{d}}{\mathrm{d}t}c(\boldsymbol{q},t) = -\int_0^t \mathrm{d}\tau\, \xi(\boldsymbol{q},t-\tau)c(\boldsymbol{q},\tau). \tag{4.57}$$

For the following discussions it is useful to consider the Laplace transformed memory function equation, which may be solved for $\hat{c}(s,\boldsymbol{q}) = \int_0^\infty \mathrm{d}t\, \exp(-st)c(t,\boldsymbol{q})$,

$$\hat{c}(s,\boldsymbol{q}) = \frac{S(\boldsymbol{q})}{s + \hat{\xi}(s,\boldsymbol{q})}, \tag{4.58}$$

as well as for $\hat{\xi}(s,\boldsymbol{q})$,

$$\hat{\xi}(s,\boldsymbol{q}) = \frac{S(\boldsymbol{q})}{c(s,\boldsymbol{q})} - s. \tag{4.59}$$

Here it has been used that $S(\boldsymbol{q}) = c(\boldsymbol{q},0)$ is the static structure factor. Eqn. (4.58) has been the starting point for the the development of many analytical models.[37] If we set $\xi(\boldsymbol{q},t) = Dq^2\delta(t)$ ($q = |\boldsymbol{q}|$), the Laplace transform is a constant in $s$, $\hat{\xi}(\boldsymbol{q},s) = Dq^2$, and it follows from eqn. (4.58) by inverse Laplace transformation,

$$\frac{c(\boldsymbol{q},t)}{S(\boldsymbol{q})} = \oint_{\mathrm{C}} \mathrm{d}s \frac{\exp(st)}{s + \hat{\xi}(s,\boldsymbol{q})} = \exp(-Dq^2t). \tag{4.60}$$

This corresponds to the Vineyard approximation for the coherent intermediate scattering function, $c(\boldsymbol{q},t) = c(\boldsymbol{q},0)c_s(\boldsymbol{q},t)$, where the self-correlation function, $c_s(\boldsymbol{q},t)$, describes free diffusion of a single particle. In general, any rational form of $\hat{c}(s,\boldsymbol{q})$ will lead to a multiexponential decay of $c(\boldsymbol{q},t)$.

**2. Autoregressive model.** To compute memory functions associated with the coherent scattering function one starts from the discretised version of the memory function, eqn. (4.57),

$$\frac{c(\boldsymbol{q},n+1) - c(\boldsymbol{q},n)}{\Delta t} = -\sum_{k=0}^{n} \Delta t \xi(\boldsymbol{q},n-k)c(\boldsymbol{q},k). \tag{4.61}$$

From a mathematical point of view the above relation is a recurrence relation where $c(\boldsymbol{q},n)$ is given and $\xi(\boldsymbol{q},n)$ is unknown. As we have shown in ref. 54, the problem can be solved by using autoregressive modelling of the underlying time series $\delta\rho(\boldsymbol{q},n) \equiv \delta\rho(\boldsymbol{q},n\Delta t)$ together with analytical properties of its $z$-transform. Here $\Delta t$ is the sampling time step. The reader is referred to ref. 54 for a detailed description of the algorithm and the application described here has been recently published in ref. 32.

Formally, eqn. (4.61) can be solved by one-sided $z$-transformation, which is defined as $F_>(z) = \sum_{n=0}^{\infty} z^{-n} f(n)$ for an arbitrary function $f(n) \equiv f(n\Delta t)$. One obtains

$$\Xi_>(\boldsymbol{q},z) = \frac{1}{\Delta t^2}\left(\frac{zS(\boldsymbol{q})}{C_>(\boldsymbol{q},z)} + 1 - z\right), \tag{4.62}$$

This equation is absolutely equivalent to relation (4.59). For eqn. (4.62) to be useful one needs a reliable estimate of $C_>(\boldsymbol{q},z)$. Such an estimate can be obtained from an autoregressive (AR) model for the underlying time series $\delta\rho(\boldsymbol{q},n)$,

$$\delta\rho(\boldsymbol{q},t) = \sum_{k=1}^{P} a_k(\boldsymbol{q})\delta\rho(\boldsymbol{q},t-k\Delta t) + \varepsilon(\boldsymbol{q},t). \tag{4.63}$$

Here $P$ is the order of the AR process, $a_k(\boldsymbol{q})$ are ($\boldsymbol{q}$-dependent) coefficients and $\varepsilon(\boldsymbol{q},t)$ is white noise with zero mean and variance $\sigma^2(\boldsymbol{q})$. In ref. 54 the set of coefficients $\{a_k,\sigma^2\}$ is fitted to the MD trajectory, using the Burg algorithm.[55–57] Within

the AR model $C_>(\boldsymbol{q},z)$ takes the form

$$C_>(\boldsymbol{q},z) = \sum_{k=1}^{P} \beta_k(\boldsymbol{q}) \frac{z_k(\boldsymbol{q})}{z - z_k(\boldsymbol{q})}. \tag{4.64}$$

Here $\{\beta_k(\boldsymbol{q})\}$ is a set of $P$ constants which depend parametrically on $\boldsymbol{q}$,

$$\beta_k(\boldsymbol{q}) = \frac{1}{a_P(\boldsymbol{q})} \frac{-z_k(\boldsymbol{q})^{P-1}\sigma(\boldsymbol{q})^2}{\prod_{j=l,j\neq k}^{P}(z_k(\boldsymbol{q}) - z_j(\boldsymbol{q}))\prod_{l=1}^{P}(z_k(\boldsymbol{q}) - z_l(\boldsymbol{q})^{-1})}, \tag{4.65}$$

and $z_k(\boldsymbol{q})$ is the $k$th root of the characteristic polynomial

$$p(z;\boldsymbol{q}) = z^P - \sum_{k=1}^{P} a_k(\boldsymbol{q}) z^{P-k}.$$

Expression (4.64) can now be used in expression (4.62) for the $z$-transformed memory function. The inverse transform into the time domain can be performed by polynomial division, comparing the resulting expression with the definition $\Xi_>(z) = \sum_{n=0}^{\infty} \xi(n) z^{-n}$.

All physical quantities derived from the AR model are represented in terms of the parameter set $\{a_k,\sigma\}$ or expressions derived from these coefficients. The dynamic structure factor is for example given by

$$S(\boldsymbol{q},\omega) = \frac{\Delta t \sigma^2(\boldsymbol{q})}{\left(1 - \sum_{k=1}^{P} a_k(\boldsymbol{q}) \exp[-\mathrm{i}\omega k \Delta t]\right)\left(1 - \sum_{m=1}^{P} a_m^*(\boldsymbol{q}) \exp[\mathrm{i}\omega m \Delta t]\right)}. \tag{4.66}$$

and the intermediate scattering function is obtained by the inverse $z$-transform

$$c(\boldsymbol{q},n) = \oint_{\mathrm{C}} \mathrm{d}s\, z^{n-1} C_>(\boldsymbol{q},n) \tag{4.67}$$

which leads to the discrete analogue of a multiexponential correlation function,

$$c(\boldsymbol{q},n) = \sum_{k=1}^{P} \beta_k(\boldsymbol{q}) z_k(\boldsymbol{q})^n, \quad n \geq 0. \tag{4.68}$$

One sees easily that all poles $z_k$ must be in the interior of the unit circle for $c(\boldsymbol{q},n)$ to stay bound for $n \to \infty$. This is guaranteed by the Burg algorithm. Another important point to be made here is that the AR model leads by construction to a multiexponential correlation function, which can *a priori* not represent algebraically decaying correlation functions. The largest accessible time scale can be estimated by

$$T_{\mathrm{AR}} \approx P\Delta t \tag{4.69}$$

and the smallest observable time scale is the sampling time step, $\Delta t$. As it will be shown in the following, the AR model can, however, *approximate* the algebraic behaviour of correlation functions.

**3. Results for lysozyme.** Fig. 14 shows two estimations for the coherent dynamic structure factor of lysozyme (solid lines: see explanations below) for $q = 10\ \mathrm{nm}^{-1}$, which have been obtained by AR modelling from an MD trajectory, and a fit of the model spectrum

$$S(\boldsymbol{q},\omega) = \frac{S(\boldsymbol{q})\tau_\alpha \sin(\alpha\pi/2)}{\pi|\omega\tau_\alpha|(|\omega\tau_\alpha|^\alpha + 2\cos(\alpha\pi/2) + |\omega\tau_\alpha|^{-\alpha})}, 0 < \alpha \leq 1, \tag{4.70}$$

which corresponds to a fractional Ornstein–Uhlenbeck process (broken line). The corresponding time correlation has the form

$$c(\boldsymbol{q},t) = S(\boldsymbol{q}) E_\alpha(-[t/\tau]^\alpha), \tag{4.71}$$

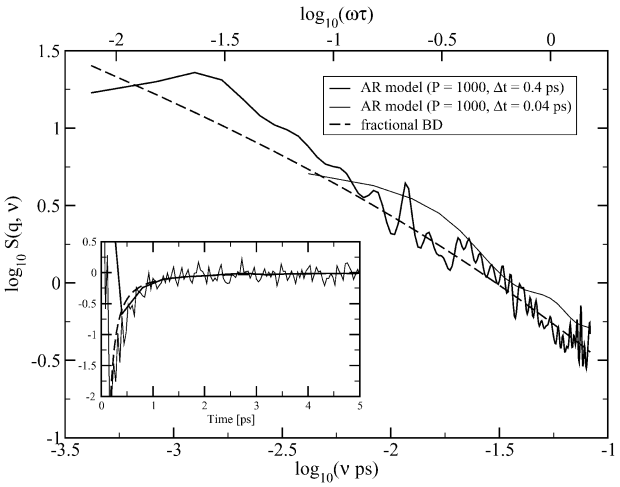


**Fig. 14** Coherent dynamic structure factor of lysozyme estimated from MD simulation and AR model (thick solid line: $P = 1000$, $\Delta t = 0.4$ ps, thin solid line: $P = 1000$, $\Delta t = 0.04$ ps) and fit of the power spectrum associated with a fractional Ornstein–Uhlenbeck process (dashed line), which has been fitted to the AR model with $P = 1000$, $\Delta t = 0.4$ ps. The inset shows the corresponding memory functions (solid lines) together with the model memory function for $t > 0$ for a fractional OU process (dashed line).

where $S(\boldsymbol{q})$ is the static structure factor. The physical interpretation of the model is that the harmonic potential defines a restoring force which tends to bring a fluctuation of the particle density back to the homogeneous density, where $\delta\rho(\boldsymbol{q},t) = 0$.

The calculations have been performed on the the basis of the same MD trajectory which has been used to compute the mean square displacement shown in Fig. 13. For the AR estimation two sets of parameters have been used: (a) $P = 1000$ with $\Delta t = 0.4$ ps (thick solid line) and (b) $P = 1000$ with $\Delta t = 0.04$ ps (thin solid line). The inset shows the corresponding memory functions. Only the data of (a) have been used for the fit of the FBD model, optimising at the same time the agreement with the Fourier spectrum and the memory function. The fitted model spectrum must be interpreted as a *trend*, allowing for oscillations due to collective motions around that trend.[32] The fit parameters, which have been obtained by setting $c(\boldsymbol{q},0) = 1$, are found to be $\tau = 2.9$ ps and $\alpha = 0.5$. The latter indicates a strongly non-exponential relaxation behaviour, as in the case of single particle relaxation dynamics which is reflected in the form of the mean-square displacement (see Fig. 13). One recognises that not only the form of the spectrum, but also the characteristic shape of the memory function are well represented by the FBD model. The clearly insufficient frequency resolution of the dynamic structure factor estimated with parameter set (b) is compensated by a memory function which is better resolved for small times and shows a remarkable overall agreement with the model memory function up to $\Delta t = 0.04$ ps. As mentioned above, the sampling time step defines the resolution of the correlation function and $T_{\mathrm{AR}} = P\Delta t$ is an estimation for the accessible time scale in the AR model. Consequently, the memory function cannot be obtained for times $t < \Delta t$ and the integral $1/\int_0^\infty \mathrm{d}t\, \xi(t)$, which defines a maximum relaxation time, cannot be infinity, as for the model memory function. Keeping the fundamental limits for the simulation results in mind, one sees that the fractional OU process is a very good model for the relaxation of the particle density towards its equilibrium value.

Since the simulation results for the dynamic structure factor and the corresponding memory function have been obtained by AR modelling of the underlying time series, it is important to verify that these estimations are reliable. Fig. 15 shows the superposition of the dynamic structure factor given in Fig. 14 (thick line) and a spectrum with has been computed by discrete

 

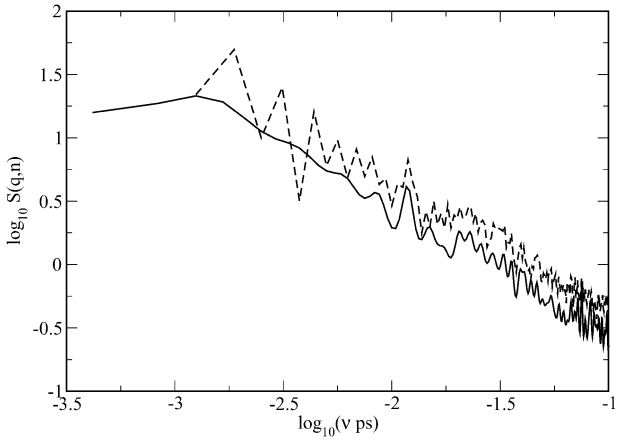


**Fig. 15** Comparison of $S_{\mathrm{coh}}(q,\omega)$ ($q = 10\ \mathrm{nm}^{-1}$) computed from AR model with $P = 1000$, $\Delta t = 0.4$ ps (solid line), and by using the standard method *via* discrete Fourier transform of a conventionally computed time correlation function (dashed line).

Fourier transform from the corresponding intermediate scattering function[58]

$$c(\boldsymbol{q},n) = \frac{1}{N_t - |n|} \sum_{j=0}^{N_t-|n|-1} \rho(\boldsymbol{q},j)^* \rho(\boldsymbol{q},j+n). \qquad (4.72)$$

Here $N_t$ is the number of time steps in the MD trajectory and $\rho(\boldsymbol{q},n)$ instead of $\delta\rho(\boldsymbol{q},n) = \rho(\boldsymbol{q},n) - \langle\rho(\boldsymbol{q},n)\rangle$ has been autocorrelated. This leads to an "elastic peak" centred at $\omega = 0$ which has been left out here. The conventionally computed spectrum in Fig. 15 is clearly more noisy than the AR spectrum. It must, however, emphasized that smoothness is not a guarantee for correctness. In order to smooth the Fourier spectrum shown in Fig. 15 the time correlation function $c(\boldsymbol{q},n)$ has been multiplied with a Gaussian window function, before performing the discrete Fourier transform. To obtain a frequency resolution comparable to the AR model a width of $\sigma = 600$ ps ($\sigma_\nu \approx 2.7 \times 10^{-4}$ THz) has been used.

### D. A coarse-grained model for protein dynamics

**1. Double harmonic approximation of the energy landscape.** In the preceding sections it has been shown that the slow relaxation dynamics at lower $q$-values can be described by a single-particle OU process with algebraic memory. Another way to describe multi-scale relaxation dynamics in proteins is to consider a *multicomponent* Ornstein–Uhlenbeck process. This has been recently demonstrated for the protein C-phycocyanin[59] (see Fig. 16), where the latter is modelled by a set of coupled Langevin oscillators which represent each a whole residue (see Fig. 17). The position of each oscillator coincides with the position of the corresponding $C_\alpha$-atom on the protein backbone. The model is inspired by Fig. 1. Each residue

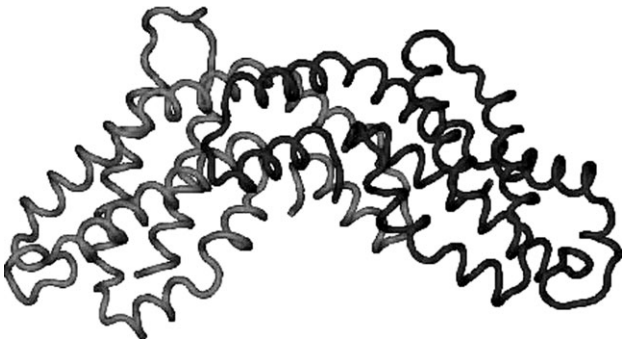

**Fig. 16** Backbone of a C-phycocyanin dimer. Shown are the chains A, B from entry 1CPC of the Brookhaven Protein Data Bank, which correspond to the simulated system analysed in ref. 59.

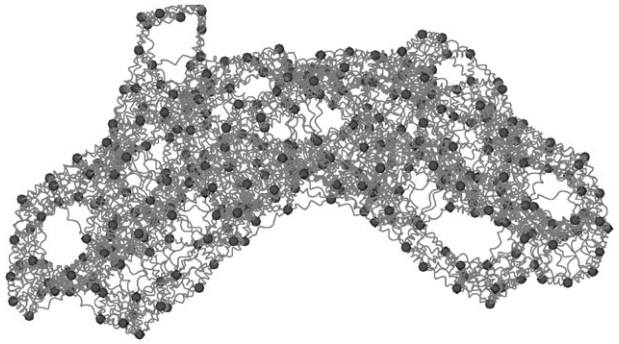

**Fig. 17** A coarse-grained model for a dimer of the C-phycocyanine molecule. Each residue is represented by a point-like Langevin oscillator (bullet), and the springs indicate harmonic coupling between the residues. More explanations are given in the text.

performs small underdamped vibrational motions in a local well and purely diffusive, strongly overdamped motions in the harmonic envelope potential. The two types of motions are supposed to be uncorrelated, such that

$$I(q,t) \approx I_{\mathrm{vib}}(q,t) I_{\mathrm{diff}}(q,t). \qquad (4.73)$$

Here the suffixes "vib" and "BD" denote, respectively, "vibrational" and "diffusion".

**2. Langevin models.** Both the local weekly damped vibrational motions and the diffusion in the harmonic envelope potential can be derived from a multi-component Ornstein–Uhlenbeck process in phase space. The corresponding Fokker–Planck equation has the form

$$\frac{\partial P}{\partial t} = A_{ij} \frac{\partial}{\partial \Omega_i} (\Omega_j P) + B_{ij} \frac{\partial^2 P}{\partial \Omega_i \partial \Omega_j}, \qquad (4.74)$$

where $\{\Omega_i\}$ ($i = 1 \ldots N$) denotes the ensemble of phase-space coordinates of $N$ Brownian particles. The latter can be represented as a $6N$-dimensional column vector $\boldsymbol{\Omega} = (\boldsymbol{x},\boldsymbol{v})$ comprising the deviations $\boldsymbol{x}$ of the Brownian particles from their respective equilibrium positions and the corresponding velocities $\boldsymbol{v}$. Correspondingly, the coefficients $\{A_{ij}\}$ and $\{B_{ij}\}$ can be represented as $6N \times 6N$ matrices $\boldsymbol{A}$ and $\boldsymbol{B}$, respectively, which have the following block structure:

$$\boldsymbol{A} = \begin{pmatrix} \boldsymbol{0} & -\boldsymbol{1} \\ \boldsymbol{\kappa} & \boldsymbol{\gamma} \end{pmatrix}, \quad \boldsymbol{B} = \begin{pmatrix} \boldsymbol{0} & \boldsymbol{0} \\ \boldsymbol{0} & k_{\mathrm{B}} T \boldsymbol{\gamma} \end{pmatrix}. \qquad (4.75)$$

Here and in the following mass-weighted coordinates are used, *i.e.* $x_i \to \sqrt{m_i} x_i$ and $v_i \to \sqrt{m_i} v_i$, with $m_i$ being the mass associated with coordinate number $i$. The matrix $\boldsymbol{\kappa}$ is derived from the second derivatives of the interaction potential $V$, evaluated at the equilibrium position $\boldsymbol{x}_{\mathrm{eq}}$,

$$\kappa_{ij} = \left.\frac{\partial^2 V}{\partial x_i \partial x_j}\right|_{\boldsymbol{x}_{\mathrm{eq}}}, \qquad (4.76)$$

and $\boldsymbol{\gamma}$ is a positive definite (mass-weighted) friction matrix. In SI units the elements of $\boldsymbol{\kappa}$ have the dimension $s^{-2}$ and those of $\boldsymbol{\gamma}$ the dimension $s^{-1}$. From a moment expansion of the Fokker–Planck equation (4.74) for a short time increment $\mathrm{d}t$ one obtains a stochastic differential equation which corresponds to the Langevin equation,

$$\frac{\mathrm{d}\boldsymbol{v}}{\mathrm{d}t} + \boldsymbol{\gamma} \cdot \boldsymbol{v} + \boldsymbol{\kappa} \cdot \boldsymbol{x} = \boldsymbol{f}_s(t). \qquad (4.77)$$

The random acceleration $\boldsymbol{f}_s(t)$ is white noise with

$$\langle \boldsymbol{f}_s(t) \rangle = \boldsymbol{0}, \quad \langle \boldsymbol{f}_s(t) \cdot \boldsymbol{f}_s^{\mathrm{T}}(t') \rangle = 2 k_{\mathrm{B}} T \boldsymbol{\gamma} \delta(t - t'). \qquad (4.78)$$

Two limits of the Langevin description are important in the following, since they describe the vibrational and the diffusional motion in the local and global harmonic potential, respectively.

(a) In the *zero friction limit* the Langevin equation becomes

$$\frac{\mathrm{d}^2\boldsymbol{x}}{\mathrm{d}t^2} + \boldsymbol{\kappa}\cdot\boldsymbol{x} = \boldsymbol{0}. \tag{4.79}$$

All static and dynamical quantities are described in terms of the normal modes $\{\boldsymbol{d}_\nu\}$ and the normal frequencies $\{\omega_\nu\}$ which are defined through

$$\boldsymbol{\kappa}\cdot\boldsymbol{d}_\nu = \omega_\nu^2\boldsymbol{d}_\nu,\ \nu = 1\ldots3N. \tag{4.80}$$

Since $\boldsymbol{\kappa}$ is positive definite, its eigenvectors form a $3N$-dimensional orthonormal basis, with $\boldsymbol{d}_\mu^{\mathrm{T}}\cdot\boldsymbol{d}_\nu = \delta_{\mu\nu}$.

(b) In the *high friction limit* the motion is strongly overdamped and the acceleration term in the Langevin equation can be neglected,

$$\boldsymbol{\gamma}\cdot\frac{\mathrm{d}\boldsymbol{x}}{\mathrm{d}t} + \boldsymbol{\kappa}\cdot\boldsymbol{x} = \boldsymbol{f}_s(t). \tag{4.81}$$

Introducing the matrices

$$\boldsymbol{\eta} = \boldsymbol{\gamma}^{-1}\cdot\boldsymbol{\kappa},\ \boldsymbol{D} = k_{\mathrm{B}}T\boldsymbol{\gamma}^{-1}, \tag{4.82}$$

the equation of motion becomes

$$\frac{\mathrm{d}\mathbf{x}}{\mathrm{d}t} + \boldsymbol{\eta}\cdot\mathbf{x} = \mathbf{v}_s(t), \tag{4.83}$$

where the random velocity $\boldsymbol{v}_s(t) = \boldsymbol{\gamma}^{-1}\cdot\boldsymbol{f}_s(t)$ has the properties

$$\langle\boldsymbol{v}_s(t)\rangle = \boldsymbol{0},\ \langle\boldsymbol{v}_s(t)\cdot\boldsymbol{v}_s^{\mathrm{T}}(t')\rangle = 2\boldsymbol{D}\delta(t-t'). \tag{4.84}$$

The Fokker–Planck description associated with the high friction limit has the form

$$\frac{\partial P}{\partial t} = \eta_{ij}\frac{\partial}{\partial x_i}(x_j P) + D_{ij}\frac{\partial^2 P}{\partial x_i\partial x_j}. \tag{4.85}$$

In a similar way as the normal modes describe the vibrational modes in the limit of vanishing friction, the eigenvectors and eigenvalues of the matrix $\boldsymbol{\eta}$, which are defined through

$$\boldsymbol{\eta}\cdot\boldsymbol{u}_\nu = \lambda_\nu\boldsymbol{u}_\nu,\ \nu = 1,\ldots,3N, \tag{4.86}$$

describe the relaxation dynamics in the high friction limit. To show the analogy with the normal modes, the eigenvectors $\boldsymbol{u}_\nu$ are called "Brownian modes" in the following. Since $\boldsymbol{\gamma}$ and $\boldsymbol{\kappa}$ are both positive definite matrices, the same is true for $\boldsymbol{\eta} = \boldsymbol{\gamma}^{-1}\cdot\boldsymbol{\kappa}$. As the normal modes, the Brownian modes thus form an orthonormal basis, $\boldsymbol{u}_\mu\cdot\boldsymbol{u}_\nu = \delta_{\mu\nu}$.

**3. Neutron scattering related quantities.** The model of coupled Langevin oscillators can be used as a basis to derive spectroscopic quantities related to neutron scattering.[60] For this purpose it is convenient to introduce dynamic form factors and to decompose the position of atom $i$ as

$$\boldsymbol{R}_i(t) = \boldsymbol{R}_i^{\mathrm{eq}} + \boldsymbol{x}_i(t), \tag{4.87}$$

where $\boldsymbol{R}_i^{\mathrm{eq}}$ is its equilibrium position and $\boldsymbol{x}_i$ the displacement with respect to $\boldsymbol{R}_i^{\mathrm{eq}}$, whose dynamics is described by a multicomponent Ornstein–Uhlenbeck process. With these definitions the dynamic form factors are defined as

$$f_{ij}(\boldsymbol{q},t) = \langle\exp(\mathrm{i}\boldsymbol{q}^{\mathrm{T}}\cdot[\boldsymbol{x}_i(t) - \boldsymbol{x}_j(0)])\rangle. \tag{4.88}$$

The intermediate scattering functions are then linear combinations of the $f_{ij}$,

$$I_{\mathrm{coh}}(\boldsymbol{q},t) = \frac{1}{N}\sum_{i,j} b_{i,\mathrm{coh}}b_{j,\mathrm{coh}}\exp(\mathrm{i}\boldsymbol{q}^{\mathrm{T}}\cdot[\boldsymbol{R}_i^{\mathrm{eq}} - \boldsymbol{R}_j^{\mathrm{eq}}])f_{ij}(\boldsymbol{q},t), \tag{4.89}$$

$$I_{\mathrm{inc}}(\boldsymbol{q},t) = \frac{1}{N}\sum_i b_{i,\mathrm{inc}}^2 f_{ii}(\boldsymbol{q},t). \tag{4.90}$$

It is convenient to write $f_{ij}(\boldsymbol{q},t)$ in the form

$$f_{ij}(\boldsymbol{q},t) = f_{ij}(\boldsymbol{q},\infty)f'_{ij}(\boldsymbol{q},t), \tag{4.91}$$

where $f_{ij}(\boldsymbol{q},\infty)$ is a static average which is described by the properties of the force constant matrix $\boldsymbol{\kappa}$ only. Using the normal modes $\boldsymbol{d}_\nu$ and the corresponding normal frequencies $\omega_\alpha$ defined above one has for the Langevin model

$$f_{ij}(\boldsymbol{q},\infty) = \exp\left(-\frac{k_{\mathrm{B}}T}{2}\sum_{\nu=1}^{3N}\omega_\nu^{-2}[(\boldsymbol{d}_\nu^{\mathrm{T}}\cdot\boldsymbol{Q}^{(i)})^2 + (\boldsymbol{d}_\nu^{\mathrm{T}}\cdot\boldsymbol{Q}^{(j)})^2]\right). \tag{4.92}$$

Here the vector $\boldsymbol{Q}^{(i)}$ has the projection property

$$\boldsymbol{Q}^{(i)}\cdot\boldsymbol{x} = \boldsymbol{q}\cdot\boldsymbol{x}_i, \tag{4.93}$$

where $\boldsymbol{x}_i$ is the three-dimensional subvector of $\boldsymbol{x}$ describing the displacement of atom $i$.

Within the Langevin model the form of the functions $f'_{ij}(\boldsymbol{q},t)$ depends on the friction matrix and will be given here for the limiting cases of zero and high friction.

(a) In the limit of vanishing friction the normal modes and frequencies suffice to construct the dynamic form factors,

$$f'_{ij}(\boldsymbol{q},t) = \exp\left(\sum_{\nu=1}^{3N} 2y_{ij}^{(\nu)}(\boldsymbol{q})\cos(\omega_\nu t)\right), \tag{4.94}$$

with $y_{ij}^{(\nu)}(\boldsymbol{q})$ given by

$$y_{ij}^{(\nu)}(\boldsymbol{q}) = \frac{k_{\mathrm{B}}T}{2\omega_\nu^2}(\boldsymbol{d}_\nu^{\mathrm{T}}\cdot\boldsymbol{Q}^{(i)})(\boldsymbol{d}_\nu^{\mathrm{T}}\cdot\boldsymbol{Q}^{(j)}). \tag{4.95}$$

(b) In the high friction limit one finds instead

$$f'_{ij}(\boldsymbol{q},t) = \exp\left(\sum_{\nu=1}^{3N} y_{ij}^{(\nu)}(\boldsymbol{q})\exp(-\lambda_\nu t)\right), \tag{4.96}$$

where $y_{ij}^{(\nu)}(\mathbf{q})$ involves the Brownian modes $\boldsymbol{u}_\nu$ defined in eqn. (4.86) and the mass-weighted force constant matrix $\boldsymbol{\kappa}$,

$$y_{ij}^{(\nu)}(\boldsymbol{q}) = k_{\mathrm{B}}T\frac{(\boldsymbol{u}_\nu^{\mathrm{T}}\cdot\boldsymbol{Q}^{(i)})(\boldsymbol{u}_\nu^{\mathrm{T}}\cdot\boldsymbol{Q}^{(j)})}{\boldsymbol{u}_\nu^{\mathrm{T}}\cdot\boldsymbol{\kappa}\cdot\boldsymbol{u}_\nu}. \tag{4.97}$$

The above expressions show that the effects of friction can in general not be accounted for by introducing friction *a posteriori* for each normal mode. This approach is only valid in the limit of low friction.[60]

The long time limits of the dynamic form factors may be used to express the EISF *via*

$$\mathrm{EISF}(\boldsymbol{q}) = \frac{1}{N}\sum_i b_{i,\mathrm{inc}}^2\exp\left(-k_{\mathrm{B}}T\sum_{\nu=1}^{3N}\omega_\nu^{-2}(\boldsymbol{d}_\nu^{\mathrm{T}}\cdot\boldsymbol{Q}^{(i)})^2\right). \tag{4.98}$$

Since static thermal averages are entirely defined by the potential function, the EISF can be expressed in the normal modes and normal frequencies only.

**4. Application to C-phycocyanin.** In the following we show an application of the coarse-grained Langevin model to C-phycocyanin.[59] The essential question is here how the envelope potential is to be parametrised. In the article cited above we adopted the choice,

$$V_{\mathrm{diff}}(\boldsymbol{x}) = \lambda V_{\mathrm{vib}}(\boldsymbol{x}), \tag{4.99}$$

where $\lambda$ is a positive real number with $0 < \lambda < 1$. Here

$$V_{\mathrm{vib}}(\boldsymbol{x}) = \frac{1}{2}\boldsymbol{x}^{\mathrm{T}}\cdot\boldsymbol{\kappa}\cdot\boldsymbol{x} \tag{4.100}$$

is a harmonic potential at the residue level. Such a potential must first be constructed from an all-atom force field, such as Amber94.[51] The details of such a method are described in ref. 59. Eqn. (4.99) stipulates that the envelope potential has exactly the same form as the local potential, and $0 < \lambda < 1$ corresponds to a global softening of $V_{\mathrm{diff}}(\boldsymbol{x})$ with respect to $V_{\mathrm{vib}}(\boldsymbol{x})$. In principle $V_{\mathrm{vib}}(\boldsymbol{x})$ must be constructed for each protein. To circumvent this problem the following approach has been suggested in ref. 59: The matrix $\boldsymbol{\kappa}$ is explicitly constructed for a small protein, crambin. In a second step we assumed that one can construct a generic force field of the form

$$V(\boldsymbol{x}) = \frac{1}{2}\sum_{ij} k(\boldsymbol{R}_{ij}^{\mathrm{eq}})(|\boldsymbol{R}_{ij}^{\mathrm{eq}} + \boldsymbol{x}_{ij}| - |\boldsymbol{R}_{ij}^{\mathrm{eq}}|)^2. \qquad (4.101)$$

Splitting according to eqn. (4.87) the position of each residue into the equilibrium position $\boldsymbol{R}_i^{\mathrm{eq}}$ and a deviation from the latter, $\boldsymbol{x}_i$, we define $\boldsymbol{R}_{ij}^{\mathrm{eq}} = \boldsymbol{R}_j^{\mathrm{eq}} - \boldsymbol{R}_i^{\mathrm{eq}}$ and $\boldsymbol{x}_{ij} = \boldsymbol{x}_j - \boldsymbol{x}_i$. We found the empirical law $k(r) \propto r$ for close distances up to 0.4 nm, and $k(r) \propto r^{-6}$ for larger distances. It is interesting to note that $r =$ 0.4 nm corresponds to the distance between two consecutive $C_\alpha$-atoms in a polypeptide chain.

The second essential input to the model is the friction matrix. For the results presented here, each residue was assigned a friction constant, assuming thus a diagonal friction matrix. For each residue the mean-square displacement of a single Langevin oscillator was fitted to the mean square displacement computed from the same MD trajectory. We found that the friction constants obtained in this way are roughly proportional to the atomic density around the respective residue. Combining this finding with the empirical harmonic force law described above, we have thus obtained a "transferable" Langevin model which does not need to be re-parametrised for each protein. As a consequence of the impact of the atomic density on the residue friction constants one observes that friction inside a protein is stronger than at the protein surface, where the residues are in contact with water, which has a lower atomic density than a protein.

Fig. 18 shows the incoherent intermediate scattering function for the $C_\alpha$-atoms in C-phycocyanine obtained by direct calculation from MD simulation, as compared to the corresponding result obtained from the model of coupled Langevin oscillators. The intermediate scattering function has been decomposed as indicated in eqn. (4.73). In order to account for a finite lifetime of the motions in a local potential minimum, we modified the corresponding dynamic form factors for vibrational motion as follows,

$$f'_{ij}(\boldsymbol{q}, t) = \exp\left(\sum_{\nu=1}^{3N} 2y_{ij}^{(\nu)}(\boldsymbol{q})\cos(\omega_\nu t)w(t)\right). \qquad (4.102)$$

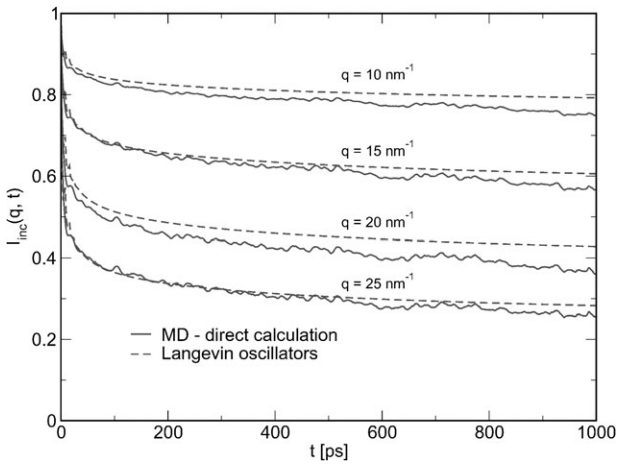


**Fig. 18** Intermediate incoherent scattering function for the $C_\alpha$ atoms in C-phycocyanine by direct calculation from MD simulation (solid line) and from the model of coupled Langevin oscillators (dashed line).

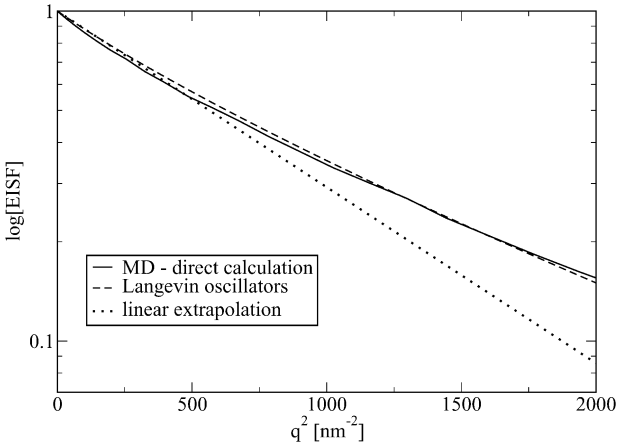


**Fig. 19** EISF corresponding to Fig. 18. The dotted line represents a linear extrapolation of $\ln(\mathrm{EISF})(q^2)$ from small $q$-values.

Here $w(t) = \exp(-[t/\tau]^2)$ is a Gaussian window function, where $\tau$ describes the lifetime of the vibrations. The steep initial decrease of the total intermediate scattering function could be adjusted with $\tau \approx 20$ ps. The scaling constant $\lambda$ in eqn. (4.99) was fitted such as to match the corresponding EISFs shown in Fig. 19. We found $\lambda = 0.115$. Although the local and the global potential surface are *a priori* not related, the fit is remarkably good and indicates a self-similarity of the structure of the energy landscape in proteins. It is also worth noting that $\ln(\mathrm{EISF})(q^2)$ is not linear, as this is the case for Gaussian single particle models, such as the OU process, which lead to a Gaussian form for the intermediate scattering function and the corresponding EISF. In contrast to a single particle model, the simulation-based model of many coupled Langevin oscillators can account for motional heterogeneity. This is easily seen from expression (4.98), where each particle contributes a Gaussian function in $q$ with a different width, such that the average is not Gaussian anymore. This apparent non-Gaussian behaviour must be distinguished from real non-Gaussian behaviour, as it is obtained for rotational diffusion models.[39] Although a number of quite drastic simplifications has been made to parametrise the Langevin oscillator model, the model is remarkably close to reality, which means that the essential features are still captured. In contrast to the models involving memory functions, multiscale relaxation is here described by coupling *many* degrees of freedom. Fig. 20 (solid line and diamonds) shows the distribution of the inverse relaxation times

$$\tau_\nu^{-1} = \lambda_\nu \qquad (4.103)$$

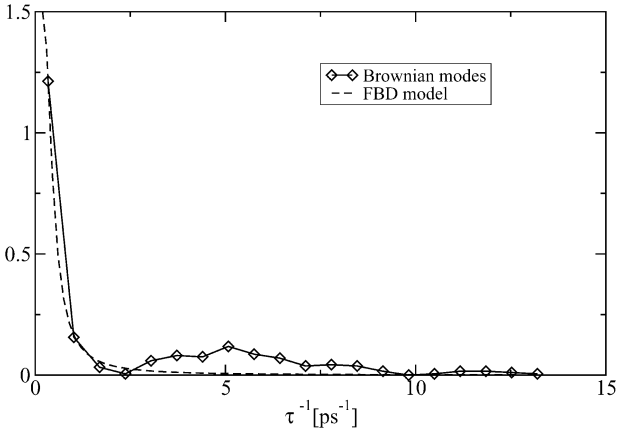


**Fig. 20** Inverse relaxation times corresponding to the intermediate scattering function depicted in Fig. 18 (solid line and diamonds) and fitted relaxation spectrum corresponding to a fractional OU process (dashed line). The resulting parameters are here $\tau = 2.98$ ps and $\alpha = 0.76$.

which are nothing but the eigenvalues $\lambda_\nu$ of the drift matrix $\boldsymbol{\eta}$ defined in eqn. (4.82). They describe the relaxation of the position correlation matrix

$$\mathbf{c}(t) = \langle \boldsymbol{x}(0) \cdot \boldsymbol{x}^{\mathrm{T}}(t) \rangle \tag{4.104}$$

from which the dynamic form factors $f'_{ij}(\boldsymbol{q},t)$, eqn. (4.96), are formally computed *via* $f'_{ij}(\boldsymbol{q},t) = \exp(\boldsymbol{Q}^{(i)\mathrm{T}} \cdot \boldsymbol{c}(t) \cdot \boldsymbol{Q}^{(j)})$. It should be noted that the histogram exhibits a strong increase for small inverse relaxation times, indicating that no maximum relaxation time can be observed within the simulation time span.

**5. Relaxation spectra.** To establish a relation between the relaxation spectrum for coupled Brownian oscillators presented in Fig. 20 and the corresponding quantity for the fractional Ornstein–Uhlenbeck process, we write the (normalised) correlation function associated with the latter in the form

$$\psi(t) = \int_0^\infty \mathrm{d}\lambda\, p(\lambda) \exp(-\lambda t). \tag{4.105}$$

Here $p(\lambda) \geq 0$ and it follows from $\psi(0) = 1$ that $p(\lambda)$ is normalised,

$$\int_0^\infty \mathrm{d}\lambda\, p(\lambda) = 1. \tag{4.106}$$

Using the definition of the Laplace transform, one finds that

$$\hat{\psi}(s) = \int_0^\infty \mathrm{d}\lambda \frac{p(\lambda)}{s+\lambda}. \tag{4.107}$$

Formally, the relation between $\hat{\psi}(s)$ and $p(\lambda)$ is a Stieltjes transform, which may be inverted to give[61]

$$p(\lambda) = \lim_{\varepsilon \to 0^+} \frac{1}{\pi} \Im\{\hat{\psi}(-[\lambda + \mathrm{i}\varepsilon])\}. \tag{4.108}$$

In case of exponential decay, where $\psi(t) = \exp(-[t/\tau])$, one has $\hat{\psi}(s) = 1/(s + \tau^{-1})$ and $p(\lambda) = \delta(\lambda - \tau^{-1})$ contributes a single inverse relaxation time, $\lambda = \tau^{-1}$. In the case of the fractional OU process one has instead

$$\hat{\psi}(s) = \frac{1}{s(1 + [s\tau]^{-\alpha})}, \quad 0 < \alpha \leq 1, \tag{4.109}$$

and the relaxation spectrum is found to be

$$p(\lambda) = \frac{\tau}{\pi} \frac{(\tau\lambda)^{\alpha-1} \sin(\pi\alpha)}{(\tau\lambda)^{2\alpha} + 2(\tau\lambda)^{\alpha} \cos(\pi\alpha) + 1}, \quad 0 < \alpha < 1. \tag{4.110}$$

The calculation is very similar to the one which leads to the Fourier spectrum presented in (2.18). Expression (4.110) coincides with the result found by Glöckle and Nonnenmacher in ref. 19, but the calculation is simpler. The dashed line in Fig. 20 shows a fit of the function (4.110) to the histogram of inverse relaxation times which has been obtained from the Brownian mode model. The fit shows a qualitative agreement for $\tau = 2.98$ ps and $\alpha = 0.76$, indicating a relaxation behaviour closer to exponential relaxation than the mean square displacement shown in Fig. 13 ($\tau = 33.5$, $\alpha = 0.49$). Here it must be kept in mind that the Brownian mode model describes protein motion on the residue level, whereas the mean square displacement in Fig. 13 contains also contributions from relaxation of very fast motions, such as side-chain rotations and vibrations. Therefore, the relaxation spectra should only be compared for small relaxation rates. The essential point is their overall agreement in this region.

## V. Conclusion

In this article it has been shown that new insights into quasielastic neutron scattering can be obtained by developing what one could call simulation-based models, where computer simulations are used as an essential input. Two approaches have been presented to describe non-exponential relaxation in a complex system like a protein: fractional Brownian dynamics of a *single* particle, and "normal" Brownian dynamics of *many* coupled particles. In both cases only modest momentum transfers can be considered since both models describe a protein on a coarse-grained scale. Localised motions, such as rapid side-chain rotations, cannot be described within these models. Roughly speaking, the concept of fractional Brownian dynamics leads to the introduction of generalized Lorentzians, which describe empirically to the very broad QENS spectra obtained from internal protein dynamics. The example of the fractional OU process has shown that the QENS spectra can be quite well reproduced with essentially one additional parameter compared to the fit of a Lorentzian. In contrast to the Kohlrausch-Williams-Watt model, where correlation functions are empirically described by stretched exponentials, the fractional OU process leads to a correlation function whose Fourier transform has a quite simple analytical form and possesses moreover a well-defined memory function.[32] The latter model has thus advantages from a practical and a theoretical point of view, although it must be clearly stated that its is still empirical at this stage. The study of the average mean square displacement of the atoms in Lysozyme has shown that FBD models may be used to extrapolate the dynamics in a certain way to very long time scales, or equivalently to low frequencies. In this respect FBD models describe what is called in mode coupling theory the "α-regime" of the dynamic structure factor, describing the slow relaxation processes.[62] It will be interesting to exploit the extrapolation properties of FBD models in combination with computer simulations to gain more insight into the influence of temperature and pressure onto the slow relaxation processes in proteins, in particular to establish a signature of protein function in these processes. A more practical question which can be addressed in this context is how elastic and quasielastic neutron scattering experiments on systems with a vast spectrum of time scales must be interpreted in view of the fact that these techniques work with a relatively small time window.[63]

Clearly, some effort has to be made now to develop a physical picture of fractional Brownian dynamics and also to make a closer contact with mode coupling theory. Here computer simulation will certainly be crucial. The model of coupled Langevin oscillators gives a hint that FBD in proteins may be formally obtained by coupling a very large number of viscoelastic elements. Such models can indeed explain "fractional" responses of end-to-end distances in polymers due to external forces.[64] It must be clearly stated that fractional BD, with absolutely no characteristic time scale, is certainly an idealized mathematical model of a physical system which has a very broad, but limited distribution of relaxation times. This point can be illustrated by the simulation study of lysozyme, which revealed a signature of fractional BD in the collective dynamics of this protein. Here the underlying time series of the Fourier transformed particle density has been modelled with a large but necessarily finite number of up to 1000 coefficients, corresponding to 1000 relaxation times. An important aspect of the computer experiment is that not only the Fourier spectrum of intermediate scattering function can be fitted by the FBD model, but also the memory function. Such a coincidence is far from being trivial. A certainly very optimistic interpretation of such computer experiments is that protein dynamics around the native state, which does not exhibit rare transitions from one global minimum to another, is essentially already developed on the nanosecond time scale, although the total relaxation may take much longer.

 

## Appendix A: $S(q,\omega)$ for the Ornstein–Uhlenbeck process

To derive the dynamic structure factor belonging to the intermediate scattering function (3.44), one uses that the latter is of the form $f(t) = \exp(-a)g(t)$, where

$$g(t) = \exp(a\,\exp(-t)), \qquad (1.1)$$

$a = q^2\langle x^2\rangle$, and $\eta t \to t$ is a dimensionless time. Since $I(q,t)$ is a classical correlation function, it is even in time, and one can stipulate $g(-t) = g(t)$. Therefore the Fourier transform of $g(t)$ is given by $\tilde{g}(\omega) = 2\Re\{\hat{g}(i\omega)\}$, where $\hat{g}(s) = \int_0^\infty \mathrm{d}t\,\exp(-st)g(t)$ is the Laplace transform of $g(t)$. By substituting $u = a\exp(-t)$ one finds that

$$\hat{g}(s) = (-a)^{-s}\,\gamma(s,-a), \qquad (1.2)$$

where $\gamma(s,a)$ is the incomplete gamma function,[30]

$$\gamma(s,a) = \int_0^a \mathrm{d}u\,\exp(-u)u^{s-1}, \quad \Re\{s\} > 0. \qquad (1.3)$$

It follows thus that

$$\tilde{f}(\omega) = \exp(-a)2\Re\{a^{-\mathrm{i}\omega}\,\gamma(\mathrm{i}\omega,-a)\}, \qquad \omega \neq 0. \qquad (1.4)$$

Using that $S(\omega) = \tilde{I}(\omega)/(2\pi)$ (the $q$-dependence is omitted) and applying the scaling law of the Laplace transform, $g(\eta t) \leftrightarrow \eta^{-1}\hat{g}(s\eta^{-1})$, one obtains expression (3.48). It is important to note that $\tilde{g}(\omega)$ does not exist for $\omega = 0$, since $\gamma(s,a)$ is defined only if $\Re\{s\} > 0$. Therefore one must define $\tilde{g}(\omega) = \lim_{\varepsilon\to 0^+} 2\Re\{\hat{g}(\mathrm{i}\omega + \varepsilon)\}$, or exclude $\omega = 0$. The value at $\omega = 0$ is not important anyway, since the elastic line, $\exp(-a)\delta(\omega)$, which completes the spectrum, is a Dirac distribution.


## Acknowledgements

The author gratefully acknowledges useful discussions with Dr K. Hinsen.


## References


1 H. Yang, G. Luo, P. Karnchanaphanurach, T. Louie, I. Rech, S. Cova, L. Xun and X. Xie, *Science*, 2003, **302**(5643), 262–266.
2 M. Ferrand, A. Dianoux, W. Petry and J. Zaccai, *Proc. Natl. Acad. Sci. USA*, 1993, **90**, 9668–9672.
3 W. Doster, S. Cusack and W. Petry, *Nature*, 1989, **337**, 754–756.
4 A. Filabozzi, A. Deriu and C. Andreani, *Physica B*, 1996, **226**, 56–60.
5 J. Fitter, *Biophys. J.*, 1999, **76**, 1034–1042.
6 J. Fitter, S. Verclas, R. Lechner, H. Seelert and N. Dencher, *FEBS Lett.*, 1998, **433**, 321–325.
7 J. Fitter, R. Lechner and N. Dencher, *J. Phys. Chem. B*, 1999, **103**, 8036–8050.
8 L. Cordone, M. Ferrand, E. Vitrano and G. Zaccai, *Biophys. J.*, 1999, **76**, 1043–1047.
9 G. Zaccai, *Science*, 2000, **288**, 1604–1607.
10 J. Fitter, R. Lechner, G. Buldt and N. Dencher, *Proc. Natl. Acad. Sci. USA*, 1996, **93**, 7600–7605.
11 J.-M. Zanotti, M.-C. Bellissent-Funel and J. Parello, *Biophys. J.*, 1999, **76**, 2390–2411.
12 S. Dellerue, A. Petrescu, J. Smith and M.-C. Bellissent-Funel, *Biophys. J.*, 2001, **81**, 1666–1676.
13 J.-M. Zanotti, J. Parello and M.-C. Bellissent-Funel, *App. Phys. A*, 2002, **74**, 1277–1279.
14 J. Pérez, J.-M. Zanotti and D. Durand, *Biophys. J.*, 1999, **77**, 454–469.
15 F. Volino and A. Dianoux, *Mol. Phys.*, 1980, **41**(2), 271–279.
16 I. Köper and M.-C. Bellissent-Funel, *App. Phys. A*, 2002, **74**(1), 1257–1259.
17 H. Yang and X. Xie, *J. Chem. Phys.*, 2002, **117**(24), 10965–10979.
18 B. Mandelbrot and J. van Ness, *SIAM Rev.*, 1968, **10**(4), 422–437.
19 W. Glöckle and T. Nonnenmacher, *Biophys. J.*, 1995, **68**, 46–53.
20 R. Metzler, E. Barkai and J. Klafter, *Phys. Rev. Lett.*, 1999, **82**(18), 3563–3567.
21 E. Barkai and R. Silbey, *J. Phys. Chem. B*, 2000, **104**, 3866–3874.
22 M. R. and J. Klafter, *Phys. Rev. E*, 2000, **61**(6), 6308–6311.
23 R. Metzler and J. Klafter, *Phys. Rep.*, 2000, **339**, 1–77.
24 E. Barkai, Y. Jung and R. Silbey, *Phys. Rev. Lett.*, 2001, **87**(20), 207403.
25 W. Coffey, Y. P. Kalmykov and J. Waldron, *The Langevin equation, Vol. 14 of World Scientific Series in Chemical Physics*, World Scientific, 2004.
26 H. Risken, *The Fokker–Planck Equation*, Springer Series in Synergetics, Springer, Berlin, Heidelberg, New York, 2nd reprinted edn., 1996.
27 N. van Kampen, *Stochastic Processes in Physics and Chemistry*, North Holland, Amsterdam, revised edn. 1992.
28 C. Gardiner, *Handbook of Stochastic Methods*, Springer Series in Synergetics, Springer, Berlin,Heidelberg, New York, 2nd edn., 1985.
29 K. Oldham and J. Spanier, *The Fractional Calculus*, Academic Press, New York, London, 1974.
30 M. Abramowitz and I. Stegun, *Handbook of Mathematical Functions*, Dover Publications, New York, 1972.
31 A. Erdélyi, W. Magnus, F. Oberhettinger and F. Tricomi, *Higher Transcendental Functions*, McGraw Hill, New York, 1955.
32 G. Kneller and K. Hinsen, *J. Chem. Phys.*, 2004, **121**(20), 10278–10283.
33 H. Frauenfelder, F. Parak and R. Young, *Ann. Rev. Biophys. Chem.*, 1988, **17**, 451–479.
34 G. Williams and D. Watts, *Trans. Faraday Soc.*, 1969, **66**, 80–85.
35 R. Bergman, *J. Appl. Phys.*, 2000, **88**(3), 1356–1365.
36 R. Zwanzig, *Lectures in Theoretical Physics*, Wiley-Interscience, New York, 1961, pp. 106–141.
37 J. Boon and S. Yip, *Molecular Hydrodynamics*, McGraw Hill, 1980.
38 S. Lovesey, *Theory of Neutron Scattering from Condensed Matter*, Clarendon Press, Oxford, 1984, **vol. I**.
39 M. Bée, *Quasielastic Neutron Scattering: Principles and Applications in Solid State Chemistry, Biology and Materials Science*, Adam Hilger, Bristol, 1988.
40 G. Kneller and J. Smith, *J. Mol. Biol.*, 1994, **242**, 181–185.
41 A. Rahman, *Phys. Rev., Sect. A*, 1964, **136**(2), 405–411.
42 G. Ciccotti, D. Frenkel and I. McDonald, *Simulation of Liquids and Solids*, North Holland, Amsterdam, 1987.
43 M. Allen and D. Tildesley, *Computer Simulation of Liquids*, Oxford University Press, Oxford, 1987.
44 D. Frenkel and B. Smit, *Understanding Molecular Simulation*, Academic Press, London, 1996.
45 G. Kneller, *Mol. Phys.*, 1994, **83**(1), 63–87.
46 *Neutrons and Numerical Methods, Vol. 479 of AIP 37 conference proceedings*, eds. G. Kearley, H. Büttner and M. Johson, American Institute of Physics, 1998.
47 M. Tarek, D. Neumann and D. Tobias, *Chem. Phys.*, 2003, **292**, 435–443.
48 M. Tarek, G. Martyna and D. Tobias, *J. Am. Chem. Soc.*, 2000, **122**, 10450–10451.
49 M. Tarek and D. Tobias, *Biophys. J.*, 2002, **79**(6), 3244–3257.
50 J. Smith, *Q. Rev. Biophys.*, 1991, **24**(3), 227–291.
51 W. Cornell, P. Cieplak, C. Bayly, I. I. R. Gould, K. Merz Jr., D. Ferguson, D. Spellmeyer, T. Fox, J. Caldwell and P. Kollman, *J. Am. Chem. Soc.*, 1995, **117**, 5179.
52 V. Hamon, *Influence de la pression sur la dynamique du lysozyme en solution, par simulation numérique et diffusion de neutrons*, PhD thesis, Université d'Orléans, 2004.
53 G. Kneller, *Mol. Sim.*, 1991, **7**, 113–119.
54 G. Kneller and K. Hinsen, *J. Chem. Phys.*, 2001, **115**(24), 11097–11105.
55 J. Burg, *Maximum entropy spectral analysis*, PhD Thesis, Stanford University, 1975, 5.
56 A. Papoulis, *Probablity, Random Variables, and Stochastic Processes*, McGraw Hill, New York, 3rd edn., 1991.
57 S. Haykin, *Adaptive Filter Theory*, Prentice Hall, 1996.
58 T. Rog, K. Murzyn, K. Hinsen and G. Kneller, *J. Comput. Chem.*, 2003, **24**(5), 657–667.
59 K. Hinsen, A.-J. Petrescu, S. Dellerue, M. Bellissent-Funel and G. Kneller, *Chem. Phys.*, 2000, **261**, 25–38.
60 G. Kneller, *Chem. Phys.*, 2000, **261**, 1–24.
61 J. Schwarz, *J. Math. Phys.*, 2005, **46**, 13501.
62 W. Doster, S. Cusack and W. Petry, *Phys. Rev. Lett.*, 1990, **65**(8), 1080–1083.
63 T. Becker, J. Hayward, J. Finney, R. Daniel and J. Smith, *Biophys. J.*, 2004, **87**, 1436–1444.
64 H. Schiessel and C. Friedrich, in *Applications of Fractional Calculus in Physics*, World Scientific, Singapore, 2000, pp. 331–376.